

# Myeloid cell transmigration across the CNS vasculature triggers IL-1 $\beta$ -driven neuroinflammation during autoimmune encephalomyelitis in mice

Sébastien A. Lévesque,<sup>1\*</sup> Alexandre Paré,<sup>1\*</sup> Benoit Mailhot,<sup>1</sup> Victor Bellver-Landete,<sup>1</sup> Hania Kébir,<sup>2</sup> Marc-André Lécuyer,<sup>2</sup> Jorge Ivan Alvarez,<sup>2,3</sup> Alexandre Prat,<sup>2</sup> Juan Pablo de Rivero Vaccari,<sup>4</sup> Robert W. Keane,<sup>5</sup> and Steve Lacroix<sup>1</sup>

<sup>1</sup>Centre de Recherche du Centre Hospitalier Universitaire (CHU) de Québec–Université Laval, Département de Médecine Moléculaire, Faculté de Médecine, Université Laval, Québec, QC G1V 4G2, Canada

<sup>2</sup>Centre de Recherche du Centre Hospitalier de l'Université de Montréal (CRCHUM), Département de Neurosciences, Faculté de Médecine, Université de Montréal, Montréal, QC H2X 0A9, Canada

<sup>3</sup>Department of Pathobiology, University of Pennsylvania, Philadelphia, PA 19104

<sup>4</sup>Department of Neurological Surgery, The Miami Project to Cure Paralysis and <sup>5</sup>Department of Physiology and Biophysics, Miller School of Medicine, University of Miami, Miami, FL 33136

**Growing evidence supports a role for IL-1 in multiple sclerosis and experimental autoimmune encephalomyelitis (EAE), but how it impacts neuroinflammation is poorly understood. We show that susceptibility to EAE requires activation of IL-1R1 on radiation-resistant cells via IL-1 $\beta$  secreted by bone marrow-derived cells. Neutrophils and monocyte-derived macrophages (MDMs) are the main source of IL-1 $\beta$  and produce this cytokine as a result of their transmigration across the inflamed blood-spinal cord barrier. IL-1R1 expression in the spinal cord is found in endothelial cells (ECs) of the pial venous plexus. Accordingly, leukocyte infiltration at EAE onset is restricted to IL-1R1<sup>+</sup> subpial and subarachnoid vessels. In response to IL-1 $\beta$ , primary cultures of central nervous system ECs produce GM-CSF, G-CSF, IL-6, Cxcl1, and Cxcl2. Initiation of EAE or subdural injection of IL-1 $\beta$  induces a similar cytokine/chemokine signature in spinal cord vessels. Furthermore, the transfer of Gr1<sup>+</sup> cells on the spinal cord is sufficient to induce illness in EAE-resistant IL-1 $\beta$  knockout (KO) mice. Notably, transfer of Gr1<sup>+</sup> cells isolated from C57BL/6 mice induce massive recruitment of recipient myeloid cells compared with cells from IL-1 $\beta$  KO donors, and this recruitment translates into more severe paralysis. These findings suggest that an IL-1 $\beta$ -dependent paracrine loop between infiltrated neutrophils/MDMs and ECs drives neuroinflammation.**

Multiple sclerosis (MS) is a debilitating autoimmune disease characterized by the presence of inflammatory lesions and demyelination plaques in the brain and spinal cord (Compston, 2004). The causes for MS remain elusive, but a complex interaction of environmental factors and genetic predispositions appear to be responsible. Among the latter, a high IL-1 $\beta$ /IL-1 receptor antagonist (IL-1Ra) ratio is associated with an increased risk of developing relapsing remitting MS (de Jong et al., 2002).

The IL-1 locus is divided into two distinct genes, namely *IL-1a* and *IL-1b*, both of which bind the same receptor complex composed of the IL-1 receptor type 1 (IL-1R1) and the IL-1 receptor accessory protein (IL-1RAcP;

Dinarelli, 2009). Although IL-1 $\beta$  is inducible and requires posttranslational proteolysis by inflammatory caspases (such as caspase-1 [Casp-1]) to signal via IL-1R1, IL-1 $\alpha$  is constitutively expressed and does not require proteolytic cleavage to become active (Rider et al., 2013).

Growing evidence supports a role for IL-1 in MS and its animal model experimental autoimmune encephalomyelitis (EAE). For example, IL-1 $\beta$  was detected in the lesions and cerebrospinal fluid of MS patients, and its presence correlates with cortical lesion load (Cannella and Raine, 1995; McGuinness et al., 1997; Mellergård et al., 2010; Seppi et al., 2014). Furthermore, drugs effective to treat MS, such as IFN- $\beta$ , glatiramer acetate (Copaxone), and natalizumab (Tysabri), impact IL-1 signaling (Mellergård et al., 2010; Carpintero and Burger, 2011).

In mice lacking IL-1, IL-1R1, or its downstream adaptor protein myeloid differentiation factor 88 (Myd88), EAE development and severity are compromised (Schiffenbauer et

\*S.A. Lévesque and A. Paré contributed equally to this paper.

Correspondence to Steve Lacroix: [steve.lacroix@crchul.ulaval.ca](mailto:steve.lacroix@crchul.ulaval.ca)

Abbreviations used: 2P-IVM, two-photon intravital microscopy;  $\alpha$ SMA,  $\alpha$ -smooth muscle actin; BMEC, brain-derived microvascular EC; BSCB, blood-spinal cord barrier; CNS, central nervous system; dpi, day post-immunization; DsRed, *Discosoma* red fluorescent protein; EAE, experimental autoimmune encephalomyelitis; EC, endothelial cell; eGFP, enhanced GFP; ISH, in situ hybridization; MDM, monocyte-derived macrophage; MS, multiple sclerosis; PFA, paraformaldehyde; TdT, tandem dimer Tomato.

© 2016 Lévesque et al. This article is distributed under the terms of an Attribution–Noncommercial–Share Alike–No Mirror Sites license for the first six months after the publication date (see <http://www.rupress.org/terms>). After six months it is available under a Creative Commons License (Attribution–Noncommercial–Share Alike 3.0 Unported license, as described at <http://creativecommons.org/licenses/by-nc-sa/3.0/>).

al., 2000; Matsuki et al., 2006; Sutton et al., 2006; Miranda-Hernandez et al., 2011; Lukens et al., 2012). Treatment with IL-1Ra or the soluble IL-1 scavenger receptor has protective effects in EAE (Jacobs et al., 1991; Badovinac et al., 1998; Furlan et al., 2007; Aubé et al., 2014). In contrast, central nervous system (CNS) remyelination in rodents appears to be dependent on IL-1 signaling (Mason et al., 2001; Vela et al., 2002), suggesting a dichotomous role of IL-1.

Because the IL-1 system appears to be a cornerstone of neuroinflammation and CNS repair, we sought to clarify the role of IL-1R1 signaling in EAE. In this study, we report that IL-1 $\beta$  produced by bone marrow-derived cells acts on IL-1R1 present on radiation-resistant (radioresistant) cells to initiate EAE. We identified neutrophils and a subset of monocyte-derived macrophages (MDMs) as the main source of IL-1 $\beta$  and show that these cells enhance their production of IL-1 $\beta$  after transmigration across the blood-spinal cord barrier (BSCB). We further demonstrate that IL-1R1 expression in the spinal cord is enriched in endothelial cells (ECs) forming walls of venules originating from the pial plexus and that leukocyte infiltration at EAE onset occurs in the subpial and subarachnoid spaces as well as around IL-1R1<sup>+</sup> veins. When treated with IL-1 $\beta$ , primary mouse and human CNS ECs adopt a cytokine signature that favors myeloid cell recruitment and activation. Finally, we found that the transfer of a mixture of neutrophils and monocytes onto the spinal cord dorsal surface of immunized IL-1 $\beta$  KO mice is sufficient to induce these mice into EAE-responding animals. Collectively, our data show that production of IL-1 $\beta$  by neutrophils and MDMs generates a milieu that further amplifies neuroinflammation through the recruitment and activation of effector myeloid cells in the CNS perivascular space and parenchyma.

## RESULTS

### Mice deficient in IL-1R1 or IL-1 $\beta$ , but not IL-1 $\alpha$ , are resistant to EAE

IL-1 is at or near the top of a hierarchical cytokine signaling cascade and is responsible for the initiation of many cellular responses during inflammatory diseases (Dinarello, 2011). In this study, we investigated the role of the IL-1 cytokine system in the pathogenesis of MS by using EAE. First, we investigated whether the absence of the *Il1r1*, *Il1a*, or *Il1b* gene would affect EAE development. Mice lacking IL-1R1 were highly resistant to EAE and presented a moderate incidence of disease (54%) with a late onset ( $25.0 \pm 3.0$  d post-immunization [dpi]) and a significant reduction in the loss of motor function or paralysis throughout the entire period of clinical evaluation (Fig. 1 A). In contrast, WT mice developed a normal ascending disease with a mean disease onset of  $12.6 \pm 4.2$  dpi (Table 1). These observations are in agreement with previous studies by other groups (Schiffenbauer et al., 2000; Sutton et al., 2006, 2009; Lukens et al., 2012) and thus confirm that IL-1R1 is of major importance for the induction of EAE.

IL-1 $\alpha$  and IL-1 $\beta$  equally influence EAE development (Matsuki et al., 2006). However, we revisited the study by

Matsuki et al. (2006), given that IL-1 $\alpha$  was recently identified as a damage-associated molecular pattern (DAMP) released by dying cells to induce sterile neuroinflammation (Bastien et al., 2015). We compared disease progression in *Il-1 $\alpha$ <sup>-/-</sup>* ( $n = 15$ ), *Il-1 $\beta$ <sup>-/-</sup>* ( $n = 29$ ), and WT ( $n = 30$ ) mice after active immunization with myelin oligodendrocyte glycoprotein peptide 35–55 (MOG<sub>35–55</sub>). As shown in Fig. 1 B, deletion of the *Il-1a* gene did not impact EAE onset or progression. In contrast, only 34% (10/29) of *Il-1 $\beta$ <sup>-/-</sup>* mice developed EAE (Fig. 1 C) and with a considerable delay in disease onset (mean of  $31.7 \pm 1.9$  d in *Il-1 $\beta$ <sup>-/-</sup>* mice vs.  $13.4 \pm 0.9$  d in WT mice; Table 1). The severity of clinical symptoms was also significantly reduced in *Il-1 $\beta$ <sup>-/-</sup>* mice compared with WT mice (Table 1), as measured with the maximum clinical score attained and area under the curve. Collectively, these data indicate that IL-1 $\beta$  and IL-1R1 are important for EAE development.

### IL-1 $\beta$ released from radiosensitive cells acts on IL-1R1 expressed by radioresistant cells to induce EAE

Next, we generated radiation bone marrow chimeras to examine whether deletion of IL-1-related genes from the radiosensitive (i.e., hematopoietic-derived cells) or radioresistant (i.e., tissue-resident cells) compartments affects EAE development. Irradiated *Il-1r1<sup>-/-</sup>* recipient mice transplanted with either WT or *Il-1r1<sup>-/-</sup>* bone marrow (WT  $\rightarrow$  *Il-1r1<sup>-/-</sup>* and *Il-1r1<sup>-/-</sup>*  $\rightarrow$  *Il-1r1<sup>-/-</sup>* mice, respectively) had a delayed disease onset and reduced disease severity compared with the WT  $\rightarrow$  WT control group (Fig. 1 D). Notably, some mice of the *Il-1r1<sup>-/-</sup>*  $\rightarrow$  *Il-1r1<sup>-/-</sup>* group were resistant to EAE (29% of them did not develop EAE; Table 1) and showed decreased spinal cord infiltration by CD45<sup>+</sup> leukocytes (not depicted), thus mimicking the phenotype observed in nonirradiated *Il-1r1<sup>-/-</sup>* mice with EAE. Collectively, these results suggest that IL-1R1 signaling in radioresistant cells is key for EAE induction but also support the role of IL-1R1 in the radiosensitive hematopoietic compartment once EAE is initiated.

To identify the cellular source of IL-1 $\beta$  responsible for activating IL-1R1 in tissue-resident radioresistant cells, we next investigated EAE in irradiated WT and *Il-1 $\beta$ <sup>-/-</sup>* mice transplanted with either WT or *Il-1 $\beta$ <sup>-/-</sup>* bone marrow-derived cells. *Il-1 $\beta$ <sup>-/-</sup>*  $\rightarrow$  WT mice were protected from EAE or exhibited delayed disease onset and reduced disease severity compared with WT  $\rightarrow$  WT and WT  $\rightarrow$  *Il-1 $\beta$ <sup>-/-</sup>* mice (Fig. 1 F and Table 1). These findings suggest that IL-1R1 is most likely activated by IL-1 $\beta$  released from radiosensitive cells and are in agreement with results obtained with *Il-1 $\alpha$ <sup>-/-</sup>* mice that show no significant differences in EAE incidence, onset, or progression between all four bone marrow chimeras generated by mixing cells from *Il-1 $\alpha$ <sup>-/-</sup>* and WT mice (Fig. 1 E and Table 1). However, the contribution of IL-1 $\beta$  derived from radioresistant cells cannot be completely excluded as WT  $\rightarrow$  *Il-1 $\beta$ <sup>-/-</sup>* mice developed EAE with a slight but significant delay in disease onset compared with WT  $\rightarrow$  WT mice ( $13.5 \pm 0.8$  vs.  $11.1 \pm 0.4$  dpi).

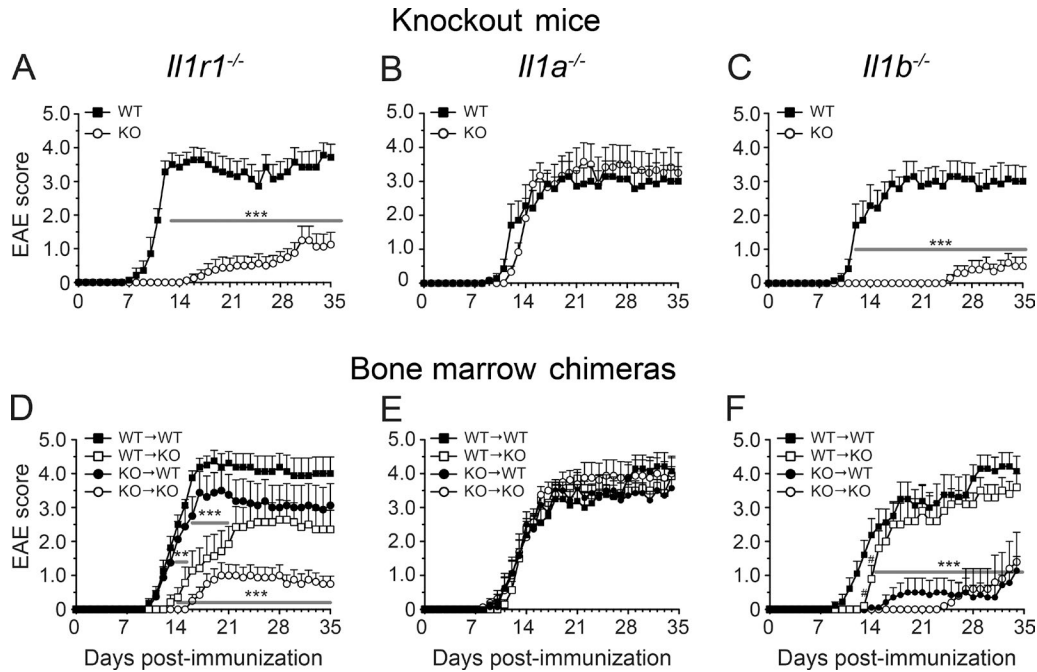


Figure 1. **IL-1 $\beta$  released from radiosensitive cells acts on IL-1R1 expressed on radioresistant cells to induce EAE.** (A–F) The clinical course of EAE was analyzed in mice constitutively lacking IL-1R1 (A;  $n = 8$ ), IL-1 $\alpha$  (B;  $n = 6$ ), or IL-1 $\beta$  (C;  $n = 10$ ) and their WT controls ( $n = 21$ ), as well as in bone marrow chimeric mice (D–F;  $n = 6$ –8/group). Results are expressed as the daily mean clinical score  $\pm$  SEM for one out of two independent experiments (details for all mice are provided in Table 1). \*\*,  $P < 0.01$ ; \*\*\*,  $P < 0.001$ , compared with WT (A–C) or WT  $\rightarrow$  WT mice (D–F), two-way repeated-measures ANOVA followed by a Bonferroni post-hoc test.

Table 1. **EAE susceptibility of mice included in this study**

Genotype	Incidence	Disease onset	AUC
<b>Constitutive KO mice</b>			
WT	22/22 (100%)	12.6 $\pm$ 4.2	39 $\pm$ 4 <sup>a</sup>
<i>Il-1r1</i> <sup>-/-</sup>	7/13 (54%)	25.0 $\pm$ 3.0	3 $\pm$ 2 <sup>a</sup>
WT	12/13 (92%)	11.8 $\pm$ 0.6	60 $\pm$ 7
<i>Il-1a</i> <sup>-/-</sup>	15/15 (100%)	12.2 $\pm$ 0.5	72 $\pm$ 7
WT	17/17 (100%)	13.4 $\pm$ 0.9	69 $\pm$ 9 <sup>b</sup>
<i>Il-1b</i> <sup>-/-</sup>	10/29 (34%)	31.7 $\pm$ 1.9	4.2 $\pm$ 2.3 <sup>b</sup>
<b>Bone marrow chimeric mice</b>			
WT $\rightarrow$ WT	8/8 (100%)	11.6 $\pm$ 0.4	89 $\pm$ 8
<i>Il-1r1</i> <sup>-/-</sup> $\rightarrow$ WT	7/7 (100%)	12.0 $\pm$ 0.8	78 $\pm$ 11
WT $\rightarrow$ <i>Il-1r1</i> <sup>-/-</sup>	6/6 (100%)	16.8 $\pm$ 1.4	52 $\pm$ 7
<i>Il-1r1</i> <sup>-/-</sup> $\rightarrow$ <i>Il-1r1</i> <sup>-/-</sup>	5/7 (71%)	17.0 $\pm$ 0.5	19 $\pm$ 5
WT $\rightarrow$ WT	15/15 (100%)	11.1 $\pm$ 0.4	79 $\pm$ 7
<i>Il-1a</i> <sup>-/-</sup> $\rightarrow$ WT	15/15 (100%)	11.6 $\pm$ 0.4	72 $\pm$ 5
WT $\rightarrow$ <i>Il-1a</i> <sup>-/-</sup>	15/15 (100%)	11.9 $\pm$ 0.2	83 $\pm$ 5
<i>Il-1a</i> <sup>-/-</sup> $\rightarrow$ <i>Il-1a</i> <sup>-/-</sup>	16/16 (100%)	11.8 $\pm$ 0.4	85 $\pm$ 5
WT $\rightarrow$ WT	15/15 (100%)	11.1 $\pm$ 0.4	79 $\pm$ 7
<i>Il-1b</i> <sup>-/-</sup> $\rightarrow$ WT	7/11 (64%)	25.6 $\pm$ 3.0	9 $\pm$ 4
WT $\rightarrow$ <i>Il-1b</i> <sup>-/-</sup>	14/14 (100%)	13.5 $\pm$ 0.8	66 $\pm$ 5
<i>Il-1b</i> <sup>-/-</sup> $\rightarrow$ <i>Il-1b</i> <sup>-/-</sup>	7/12 (58%)	25.0 $\pm$ 2.0	15 $\pm$ 5

Two independent experiments were performed, and the pooled data are shown.

<sup>a</sup>The area under the curve (AUC) was calculated up to day 28 after MOG<sub>35-55</sub> immunization.

<sup>b</sup>The AUC was calculated only for the first experiment (WT mice,  $n = 7$ ; *Il-1b*<sup>-/-</sup> mice,  $n = 10$ ), as mice included in the second experiment were killed at EAE onset + 1.

### EAE onset is supported by neutrophils and a subset of MDMs producing bioactive IL-1 $\beta$

Next, we sought to determine the timing and location for the production of bioactive IL-1 $\beta$  during EAE. Given that *IL-1b* mRNA had previously been detected in MS lesions (McGuinness et al., 1997), we measured bioactive IL-1 $\beta$  and Casp-1 by immunoblotting in homogenates of brain, spinal cord, and optic nerve collected at 0, 1, 3, 7, 10, and 14 dpi. As shown in Fig. 2 (A–C), bioactive IL-1 $\beta$  (p17) and Casp-1 (p26) were significantly increased in the lumbar spinal cord at EAE onset (day 10) and peak of the disease (day 14). The thoracic and cervical spinal cord segments showed similar patterns of IL-1 $\beta$  and Casp-1 expression (not depicted). Basal levels of IL-1 $\beta$  were also detected in the brain and optic nerve but remained unchanged at all times despite an up-regulation trend after immunization (not depicted). Because we established that increased IL-1 $\beta$  protein expression by radiosensitive cells coincides with infiltration of CD45<sup>+</sup> leukocytes in the spinal cord (Aubé et al., 2014), we next determined which leukocytes were responsible for IL-1 $\beta$  production in the CNS. To that end, we used transgenic mice expressing *Discosoma* red fluorescent protein (DsRed) under the control of the *Il1b* promoter (Matsushima et al., 2010). First, we confirmed that these mice develop EAE normally and found no differences in disease onset and EAE severity compared with their WT littermates (not depicted). We then analyzed the DsRed-expressing cells in the spinal cord at the peak of EAE (Fig. S1). Spinal cord infiltrates were mainly composed of MDMs (38  $\pm$  3%), neutrophils (16  $\pm$  3%), and T lymphocytes (19  $\pm$  2%; not depicted), values that are in line with previous findings (Steinbach et al., 2013; Lewis et al., 2014). Microglia accounted for  $\sim$ 6  $\pm$  1% of all CD45<sup>+</sup> leukocytes (not depicted). Among these four populations of CD45<sup>+</sup> cells, neutrophils (28.2  $\pm$  5.1%) and MDMs (66.2  $\pm$  5.2%) accounted for 94.4% of all DsRed-expressing cells (Fig. 2 D). DsRed<sup>+</sup> MDMs comprised >70% of MHCII<sup>+</sup> cells, with an  $\sim$ 50:50 mixture of lymphocyte antigen 6C (Ly6C)<sup>Hi</sup> and Ly6C<sup>Int</sup> cells (not depicted). On average, we found that 72.0  $\pm$  2.4% of neutrophils expressed DsRed compared with 39.9  $\pm$  2.9% of MDMs at 14 dpi (Fig. 2 E). In contrast, only 9.5  $\pm$  2.3% of microglia and 0.14  $\pm$  0.03% of T lymphocytes expressed DsRed and together only accounted for 3.9% of all IL-1 $\beta$ -producing cells (Fig. 2, D and E). Using real-time quantitative RT-PCR, we further confirmed that DsRed<sup>+</sup> neutrophils and MDMs, but not DsRed<sup>-</sup> T lymphocytes and MDMs, expressed *Il-1b* and *Casp-1* (Fig. 2 F). We then determined whether IL-1 $\beta$  expression is triggered in the CNS or if it is carried over by infiltrating myeloid cells. We found that <2% of all CD45<sup>+</sup> cells in the bone marrow of naive mice express DsRed, and this ratio did not change significantly throughout the course of EAE (Fig. 2 G). A similar proportion of DsRed<sup>+</sup> cells (3  $\pm$  1%) was found in the blood of naive mice (Fig. 2 H). However, this changed drastically during EAE as CD45<sup>+</sup> DsRed<sup>+</sup> leukocytes increased to 21  $\pm$  1% at 7 dpi before returning to baseline by day 10, paralleling the blood neutrophilia in EAE

mice (Fig. 2 H). In addition, most DsRed<sup>+</sup> cells (i.e., 80.7  $\pm$  4.1% on average) in the blood were neutrophils at all the time points studied (Fig. 2 I). Interestingly, the proportion of circulating neutrophils expressing DsRed ranged from 15 to 20% and did not significantly change after immunization (not depicted). Collectively, our observations show that neutrophils and MDMs are the main producers of IL-1 $\beta$  during EAE. Additionally, the proportion of neutrophils expressing IL-1 $\beta$  (DsRed<sup>+</sup>) increased dramatically in the spinal cord after disease onset (Fig. 2 J).

To determine the localization of infiltrated leukocytes, we analyzed spinal cord sections and quantified perivascular DsRed-expressing cells. DsRed<sup>+</sup> cells mainly stained positive for the neutrophil/MDM marker Ly6B.2 (7/4 antigen; not depicted) and the neutrophil marker lymphocyte antigen 6G (Ly6G; 67.5  $\pm$  6.5%; Fig. 3, A and D). Very few DsRed<sup>+</sup> cells expressed the T lymphocyte marker CD3 (2.5  $\pm$  0.9%), whereas 15.7  $\pm$  2.7% of them expressed the microglia/macrophage marker ionized calcium-binding adaptor molecule 1 (Iba1; Fig. 3, B–D). Interestingly, myeloid cells producing pro-IL-1 $\beta$  were consistently found in the white matter blood vessels in proximity to the meninges. Collectively, these results show that cells of the myeloid lineage, primarily neutrophils and MDMs, are the principal producers of IL-1 $\beta$  during the early phases of EAE.

### IL-1 $\beta$ expression by neutrophils is not required for their firm adhesion to spinal cord postcapillary venules during EAE

We recently showed that neutrophils systemically infused into *Il-1r1*<sup>-/-</sup> EAE mice fail to firmly adhere and migrate across the BSCB (Aubé et al., 2014). In this study, we compared the attachment of fluorescently labeled *Il-1b*<sup>-/-</sup> and WT neutrophils to venular ECs at the onset of EAE using real-time intravital imaging. We focused our study on neutrophils, as they are one of the two main sources of IL-1 $\beta$  and are easier to purify in higher numbers than monocytes. We did not find significant differences in the number of *Il-1b*<sup>-/-</sup> and WT neutrophils firmly adhering to postcapillary venules within the spinal cord of EAE mice (Fig. 4 A). This indicates that in neutrophils IL-1 $\beta$  is dispensable for their adhesion to the BSCB. Based on these results, and the undetectable levels of IL-1 $\beta$  in circulation (not depicted), we hypothesized that IL-1 $\beta$  is produced by neutrophils and MDMs upon adhesion or after transmigration into the CNS.

### Neutrophils and MDMs produce pro-IL-1 $\beta$ upon migration across the BSCB

To test this idea, we allowed Gr1<sup>+</sup> cells isolated from the bone marrow of p*Il1b*-DsRed mice to migrate across a monolayer of primary mouse brain-derived microvascular ECs (BMECs; Fig. 4 B). After 18 h, nonmigrating and migrating cells were collected and analyzed by flow cytometry. Interestingly, the percentage of transmigrated DsRed<sup>+</sup> cells was sixfold higher as compared with unmigrated cells (Fig. 4, C and D). The mean DsRed fluorescence intensity was also significantly

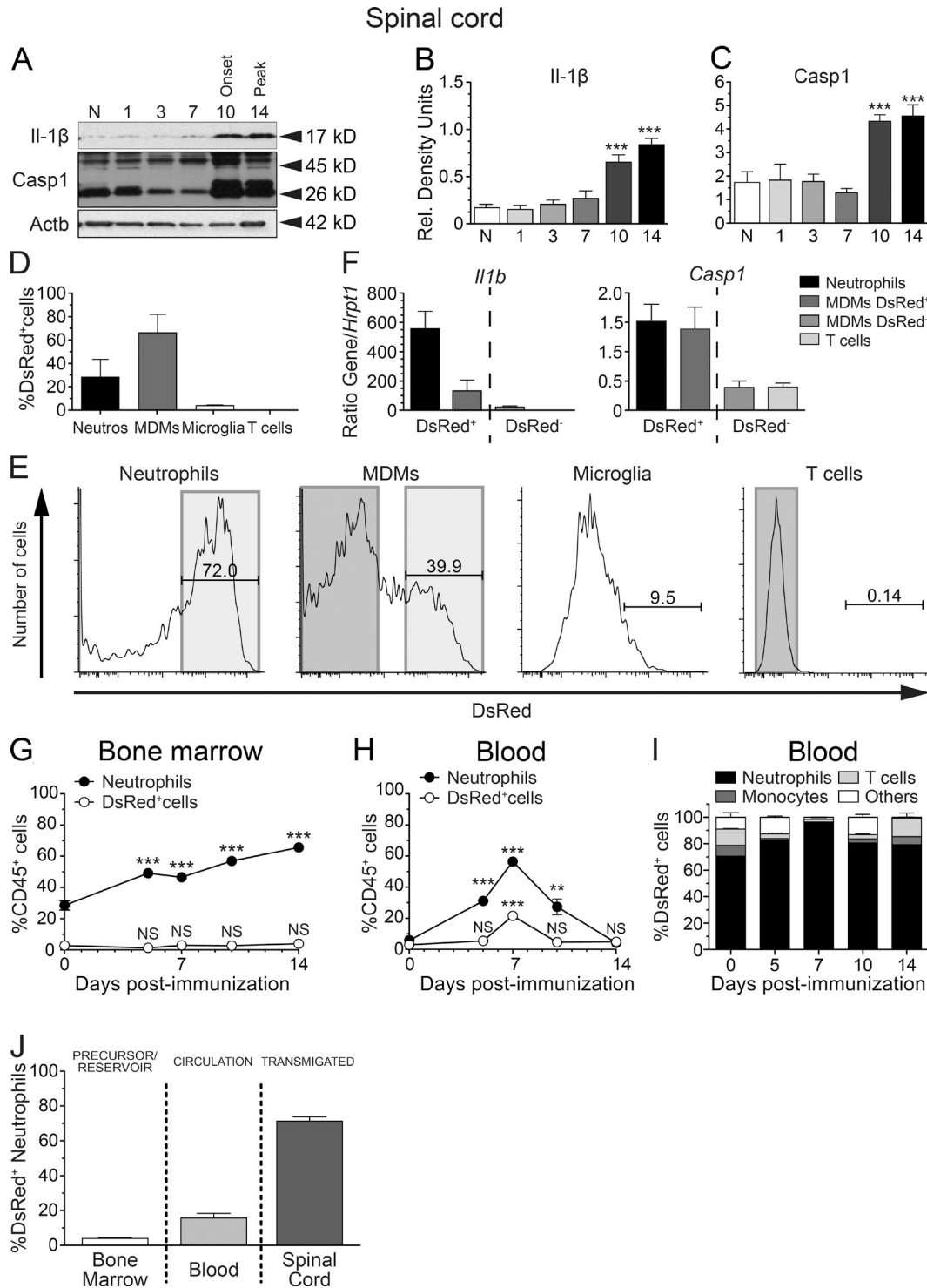


**Figure 2. Neutrophils and MDMs are the relevant IL-1 $\beta$ -producing cells in the acute phase of EAE.** (A) Representative immunoblots for bioactive IL-1 $\beta$  and Casp-1 performed on cell lysate extracts obtained from the lumbar spinal cord of EAE mice at different days after immunization. (B and C) Densitometric quantification of immunoblot revealed that the bioactive forms of IL-1 $\beta$  (p17; B) and Casp-1 (p26; C) were converted from their respective pro-forms beginning at the onset of EAE. Results were normalized with  $\beta$ -actin. (D and E) Flow cytometric analysis of whole spinal cords of *p//1b*-DsRed mice collected at 14 dpi ( $n = 4$ ). Individual leukocyte populations were immunophenotyped based on their expression (or lack thereof) of CD11b, CD3, Ly6C, and Ly6G, whereas expression of the fluorescent reporter DsRed was used to identify pro-IL-1 $\beta$ -producing cells. The percentage of all DsRed-expressing cells identified as microglia (CD45<sup>dim</sup>CD11b<sup>dim</sup>Ly6G<sup>-</sup>), T lymphocytes (CD45<sup>hi</sup>CD11b<sup>-</sup>CD3<sup>+</sup>), MDMs (CD45<sup>+</sup>CD11b<sup>+</sup>CD3<sup>-</sup>Ly6C<sup>int-hi</sup>Ly6G<sup>-</sup>), and neutrophils (CD45<sup>+</sup>CD-

higher in migrated Gr1<sup>+</sup> cells (Fig. 4 E), indicating that trans-endothelial migration triggers *Il-1β* expression. Notably, this was also found to be the case when BMECs lacking IL-1R1 were tested, although transmigration of Gr1<sup>+</sup> cells was reduced by 60% in the absence of IL-1R1 (not depicted).

Next, we performed real-time assessment of IL-1β production in the lumbar spinal cord of living EAE mice using two-photon intravital microscopy (2P-IVM). To visualize and track IL-1β production by myeloid cells, *p11b-DsRed* transgenic mice were crossed with *LysM-GFP* knock-in mice expressing enhanced GFP (eGFP) in mature cells of the granulo-myelomonocytic lineage, which mainly includes neutrophils and MDMs. Hence, by imaging these double-transgenic mice, we were able to demonstrate that CNS-infiltrated *LysM-GFP*<sup>+</sup> cells express significantly higher levels of pro-IL-1β (DsRed) than *LysM-GFP*<sup>+</sup> cells that were found circulating, rolling, or adhering to spinal cord endothelium (Fig. 4, F–H; and Videos 1 and 2), a phenomenon more predominant at disease onset (Fig. 4, G and H). The vast majority of DsRed<sup>+</sup> cells were found in the perivascular space of postcapillary venules in proximity to the spinal cord dorsal vein. These observations suggest that events occurring during the emigration through the BSCB are responsible for the induction of *Il-1β* production during EAE onset.

#### IL-1β is produced by infiltrating myeloid cells but not by resident leptomeningeal macrophages

Given that *LysM-Gfp::p11b-DsRed* mice do not allow for the discrimination between MDMs and resident leptomeningeal macrophages, we generated *CX<sub>3</sub>CR1-Cre<sup>ERT2</sup>::Rosa26-TdT* transgenic mice in which CNS-resident macrophages and microglia can be differentiated from bone marrow-derived monocytes based on the expression of the tandem dimer Tomato (TdT) reporter. *CX<sub>3</sub>CR1-Cre<sup>ERT2</sup>::Rosa26-TdT* mice received tamoxifen treatment 1 mo before experimentation to activate the inducible Cre recombinase for recombination of TdT floxed. In naive transgenic mice, TdT<sup>+</sup> cells in the spinal cord included parenchymal microglia as well as leptomeningeal macrophages found in the dura, arachnoid, and pia maters (Fig. 5 A). Having confirmed that leptomeningeal macrophages and parenchymal microglia from *CX<sub>3</sub>CR1-Cre<sup>ERT2</sup>::Rosa26-TdT* mice expressed TdT, we next examined IL-1β expression at the peak of EAE using a polyclonal anti-mouse IL-1β antibody, whose specificity was confirmed by immunostaining of tissue sections from IL-1β<sup>-/-</sup> mice (Fig. S2). As shown in Fig. 5 B, IL-1β colocalized

exclusively with CD11b<sup>+</sup> TdT<sup>-</sup> cells, indicating that bone marrow-derived myeloid cells are the main source of IL-1β. To further confirm that infiltrating myeloid cells are the main producers of IL-1β in the spinal cord, we crossed *CX<sub>3</sub>CR1-Cre<sup>ERT2</sup>::Rosa26-TdT* mice with *LysM-GFP* mice and immunized the resulting triple transgenic animals. As shown in Fig. 5 C, IL-1β immunoreactivity was seen in the majority of *LysM-GFP*<sup>+</sup> myeloid cells but not in TdT<sup>+</sup> resident cells. Collectively, our results indicate that bone marrow-derived myeloid cells, but not microglia and resident leptomeningeal macrophages, are the primary source of IL-1β in EAE.

#### IL-1R1 is mainly expressed by ECs of the pial venous plexus, and its expression correlates with primary sites of leukocyte infiltration

We next sought to identify the radioresistant cells that express IL-1R1 in the CNS. As shown in Fig. 6 A, IL-1R1 was mainly detected on ECs and in close proximity to DsRed (IL-1β)-expressing cells. Further detailed analysis of spinal cord sections from both naive and EAE mice revealed colocalization of IL-1R1 with CD31<sup>+</sup> ECs on 13 ± 5% of blood vessels, primarily those that vascularize the arachno-pial space and white matter. Interestingly, IL-1R1 appeared to be expressed mainly on the abluminal surface of ECs (Fig. 6, B–D), an intriguing finding considering that myeloid cells produce IL-1β as a result of their transmigration across the CNS endothelium. As our studies using bone marrow chimeras indicated that IL-1R1 expression on radioresistant cells promotes EAE, we next investigated IL-1R1 expression at the BSCB. We did not observe colocalization of IL-1R1 staining and the expression of the artery-specific dye Alexa Fluor 633 hydrazide (not depicted). Furthermore, IL-1R1 did not colocalize with α-smooth muscle actin (αSMA; Fig. 6 E), a pericyte/fibroblast marker associated with arteries and arterioles (Carare et al., 2008). Notably, blood vessels with a diameter <10 μm rarely stained positive for IL-1R1, suggesting that its expression was restricted to venules or veins radiating toward the pial venous plexus. IL-1R1 was not detected on cells expressing the CNS pericyte markers β-type platelet-derived growth factor receptor (PDGFR-β; Fig. 6 F), neuron-glial antigen 2 (NG2; not depicted), and desmin (not depicted). Similarly, IL-1R1 staining did not colocalize with glial fibrillary acidic protein (GFAP)-positive astrocytes and their end-feet processes (Fig. 6 G), indicating that the IL-1R1 expression is restricted to ECs. Interestingly, myeloid cell infiltration into the spinal cord of MOG-immunized *LysM-GFP* knock-in mice occurs

11b<sup>+</sup>CD3<sup>-</sup>Ly6C<sup>int</sup>Ly6G<sup>hi</sup>) is shown in D. (F) To further correlate the presence of DsRed with IL-1β, DsRed<sup>+</sup> neutrophils and MDMs, as well as DsRed<sup>-</sup> MDMs and T cells, were sorted, and *Il-1β* and *Casp-1* mRNA levels were analyzed by real-time quantitative RT-PCR. (G and H) Flow cytometric analysis of bone marrow (G) and blood (H) samples from *p11b-DsRed* mice at various days after immunization (*n* = 5 mice/time). The percentage of total neutrophils and DsRed<sup>+</sup> cells are expressed as a ratio of total CD45<sup>+</sup> leukocytes. (I) Percentage of DsRed<sup>+</sup> cells in the blood that are neutrophils, monocytes, lymphocytes, or other cells (*n* = 5 mice/time). (J) Percentage of neutrophils producing pro-IL-1β (DsRed) in the bone marrow, blood, and spinal cord at the peak of clinical score (14 dpi). All data are expressed as mean ± SEM. \*\*, *P* < 0.01; \*\*\*, *P* < 0.001, compared with naive mice; one-way ANOVA followed by Dunnett's post-hoc test (B, C, G, and H).

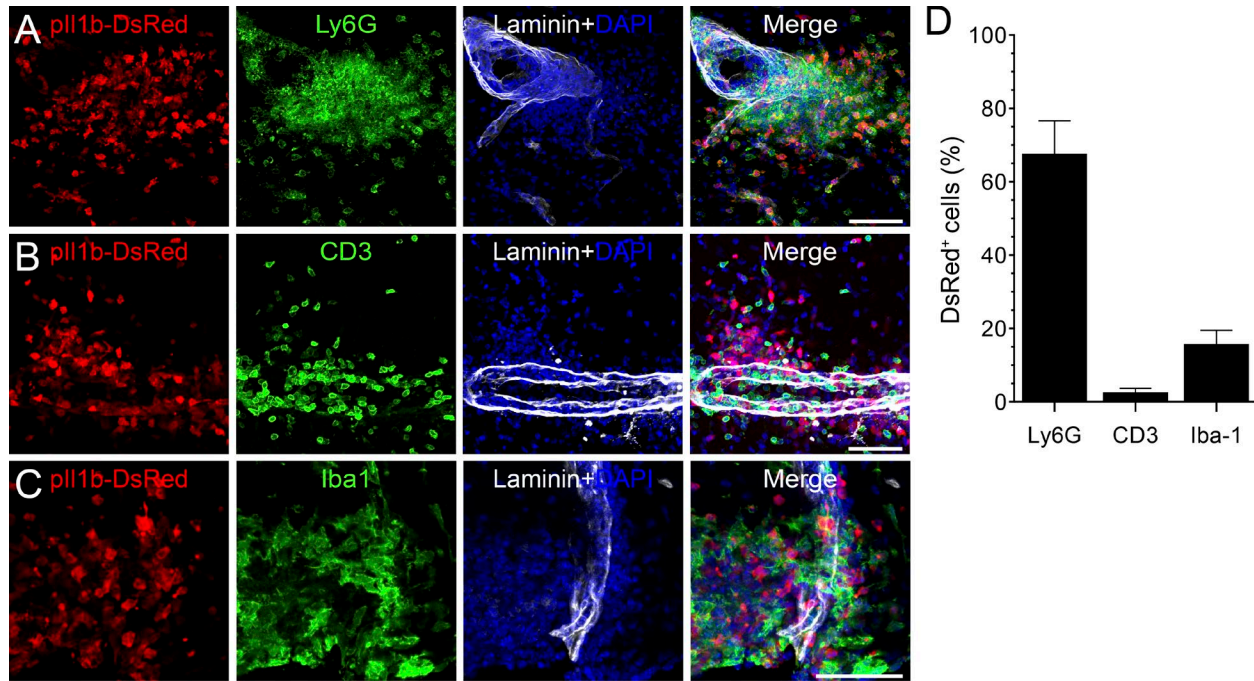


**Figure 3. IL-1 $\beta$  is mainly expressed by neutrophils and macrophages that infiltrated the spinal cord parenchyma at the peak of disease.** (A–C) Representative confocal images of *p11b*-DsRed transgenic mice at the peak of EAE showing the high density of DsRed<sup>+</sup> cells in the spinal cord parenchyma. Tissue sections were immunostained with antibodies directed against Ly6G, CD3, or Iba1 to identify neutrophils (A; green), T lymphocytes (B; green), or macrophages/microglia (C; green), respectively. An anti-pan-laminin antibody was used to stain blood vessel basement membranes (white staining). (D) Quantification of colocalization for DsRed and markers of immune cell types. Data are presented as means  $\pm$  SEM ( $n = 3$  mice; more than three sections per mouse) and are representative of two independent experiments. Bars, 100  $\mu$ m.

predominantly through IL-1R1<sup>+</sup> rather than IL-1R1<sup>-</sup> vessels (Fig. 6 H). Collectively, our results show that the radioresistant component of the induced IL-1R1 response is highly restricted to venular ECs. Because this represents the principal site of entry of myeloid cells during EAE, we next investigated whether IL-1 $\beta$  acting on CNS ECs may influence the inflammatory cascade, leading to neuroinflammation.

#### Stimulation of CNS-ECs with IL-1 $\beta$ initiates the production of proinflammatory cytokines critical to EAE/MS pathogenesis

Previous *in vitro* studies have shown that IL-1 $\beta$  triggers the production and release of several proinflammatory cytokines from ECs (Zsebo et al., 1988; Williams et al., 2008). We first determined the profile of cytokines released by primary mouse CNS-ECs after IL-1 $\beta$  stimulation. Treatment with recombinant mouse TNF + IFN- $\gamma$ , which are known to induce the cell differentiation of monocytes into T<sub>H</sub>17-polarizing APCs (Ifergan et al., 2008), was used as a control. As shown in Fig. 7 A, the IL-1 $\beta$ -driven cytokine/chemokine release was characterized by elevated amounts of IL-6 and chemokine (C-C motif) ligand 2 (Ccl2), as well as a striking increase in levels of GM-CSF, G-CSF, chemokine (C-X-C motif) ligand 1 (Cxcl1), Cxcl2, and Cxcl5. Interestingly, the cytokines and chemokines released by CNS-ECs after TNF + IFN- $\gamma$  stim-

ulation differ drastically from those released in response to IL-1 $\beta$ . Careful analysis revealed that IL-1 $\beta$  favors the release of EC-derived chemokines involved in the recruitment of neutrophils and monocytes (e.g., Cxcl1, Cxcl2, Cxcl5, and Ccl2) and that support the maturation of bone marrow-derived cells into neutrophils, monocytes, and APCs (G-CSF, GM-CSF, and IL-6). In contrast, TNF and IFN- $\gamma$  induced the systemic release of chemokines involved in the recruitment of monocytes and T lymphocytes (e.g., Cxcl9, Cxcl10, Ccl3, Ccl4, and Ccl5), as well as cytokines that promote the maturation of bone marrow-derived cells into MDMs and lymphocytes (e.g., M-CSF and IL-7). Notably, IL-1 $\beta$  did not induce the release of TNF from BMECs and vice versa (not depicted), which suggests that these two cytokines are not completely redundant and thus play complementary roles during neuroinflammation.

To ascertain whether these results reflect the *in vivo* situation, we combined *in situ* hybridization (ISH) with immunohistochemistry to determine the cellular source of IL-1 $\beta$ -driven cytokines known to be critical to EAE pathogenesis, such as GM-CSF, G-CSF, and IL-6 (Eugster et al., 1998; Okuda et al., 1998; Samoilova et al., 1998; McQualter et al., 2001; Rumble et al., 2015). We show that, at the peak of EAE, white matter CD31<sup>+</sup> ECs express *GM-CSF*, *G-CSF*, and *Il-6* mRNAs (Fig. 7, B–D). Using primary

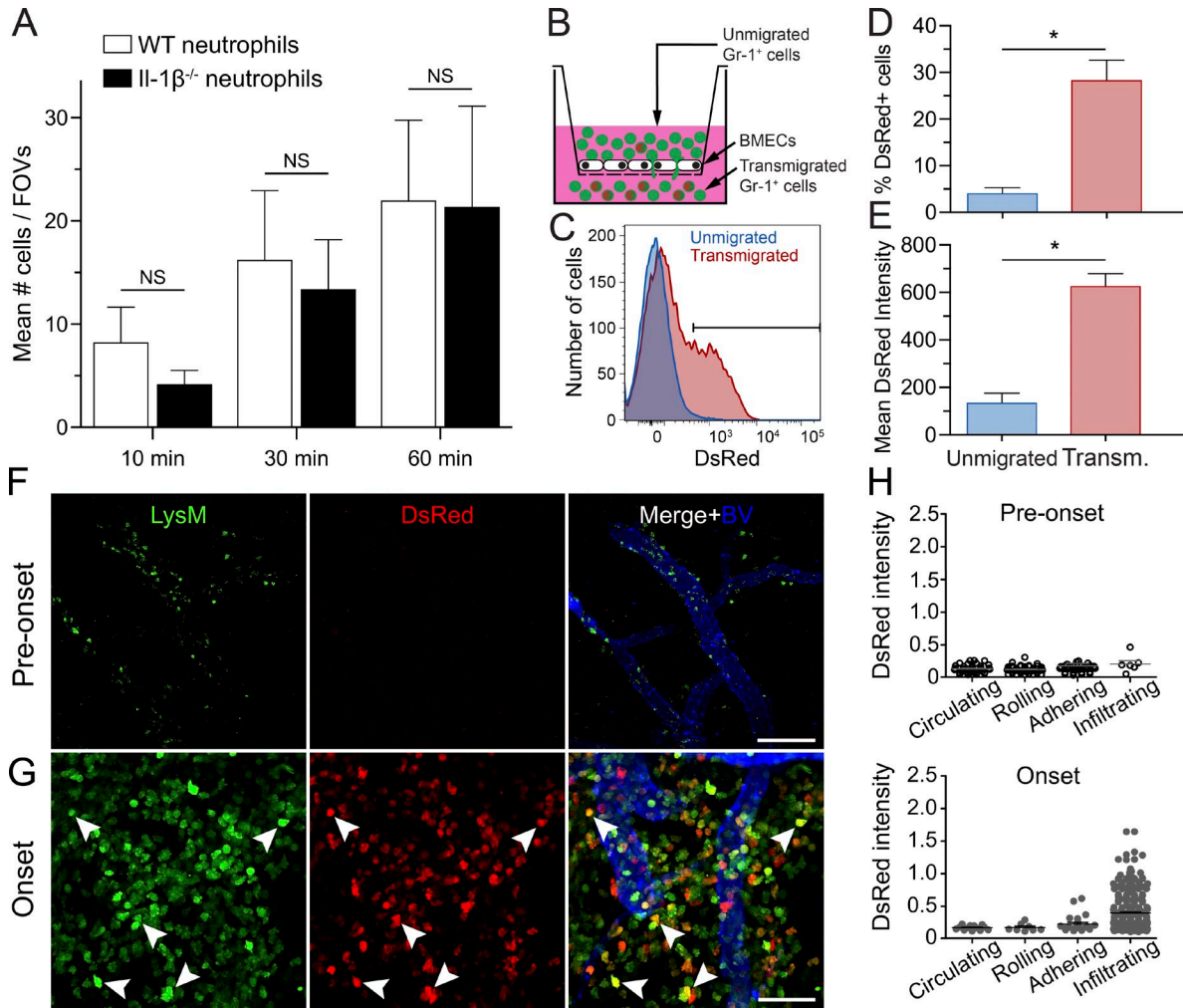


**Figure 4. IL-1 $\beta$  is produced by neutrophils and MDMs as a result of their transmigration across the BSCB.** (A) Quantification of firm neutrophil adhesion at 10, 30, and 60 min after systemic infusions of fluorescently stained WT or IL-1 $\beta^{-/-}$  neutrophils into WT recipient EAE mice ( $n = 10-12$ ). All data are expressed as means  $\pm$  SEM with the mean representing the total number of firmly adherent neutrophils in eight fields of view (FOVs). (B) Scheme of the in vitro transmigration assay in which Gr1 $^{+}$  cells were allowed to transmigrate across a confluent monolayer of BMECs. (C) Flow cytometric analysis of DsRed expression in untransmigrated and transmigrated Gr1 $^{+}$  cells. (D and E) Quantification of the percentage of DsRed-expressing cells (D) and the mean DsRed fluorescence intensity (E) in untransmigrated versus transmigrated Gr1 $^{+}$  cells. Mean  $\pm$  SEM of three independent experiments is shown. \*,  $P < 0.05$ . (F and G) 2P-IVM of the spinal cord of *LysM-GFP::p11b-DsRed* double transgenic mice 2 d before onset (F) and at onset (G). Blood vessels were visualized by i.v. injection of a 10% solution of Qdot705 (blue). Myeloid cells (*LysM-GFP $^{+}$*  cells) expressing the pro-form of IL-1 $\beta$  (DsRed signal) are shown with filled arrowheads. (H) Quantitative analysis of the DsRed fluorescence intensity (normalized to GFP fluorescence intensity) of circulating, rolling, adhering, and infiltrating (transmigrated) *LysM $^{+}$*  cells ( $n = 3$  mice/group). Means  $\pm$  SEM are shown, and data are representative of two independent experiments.

cultures of human CNS-ECs, we confirmed that IL-1 $\beta$  induces a similar cytokine signature, i.e., the release of G-CSF, GM-CSF, IL-6, and CXCL8 (IL-8; Fig. 7, E–H). Interestingly, the increased secretion of GM-CSF and G-CSF was only detected upon IL-1 $\beta$  stimulation but not with TNF + IFN- $\gamma$  (Fig. 7, E and F). No significant differences were found between unstimulated, IL-1 $\beta$ , and TNF/IFN- $\gamma$  treatment in terms of CCL2 secretion, although a trend toward increased secretion was observed for cells treated with recombinant IL-1 $\beta$  (Fig. 7 I). Because we established that IL-1R1 is constitutively expressed by a subset of blood vessels

located within the arachno-pial space and spinal cord white matter, we next determined whether a single acute subdural injection of IL-1 $\beta$  would induce a similar cytokine/chemokine expression signature in the BSCB. As shown in Fig. 7 (J and K), subdural injection of IL-1 $\beta$ , but not saline (not depicted), into naive mice resulted in strong expression of *G-CSF* and *IL-6* mRNAs in CD31 $^{+}$  blood vessels located in the white matter. These results suggest that IL-1 $\beta$ /IL-1R1 signaling in ECs lining CNS venules creates a local environment favoring the recruitment and activation of effector myeloid cells.

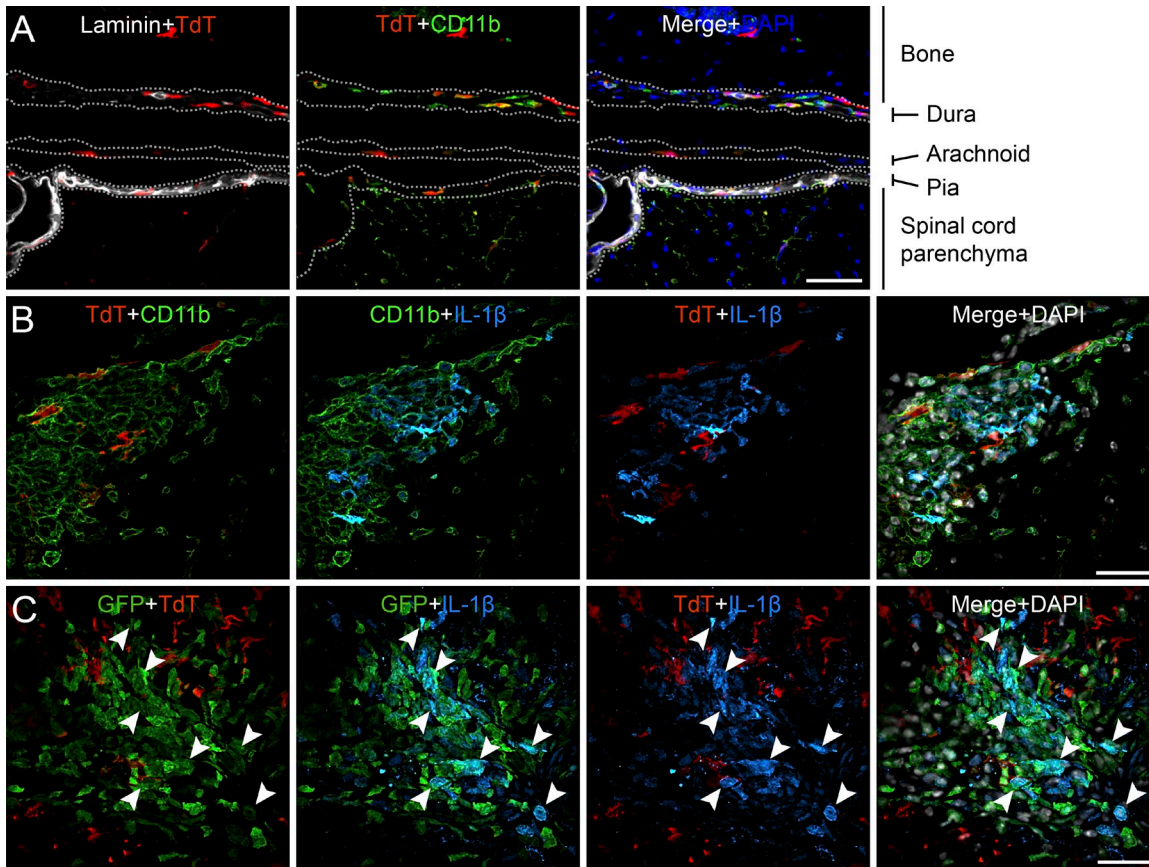
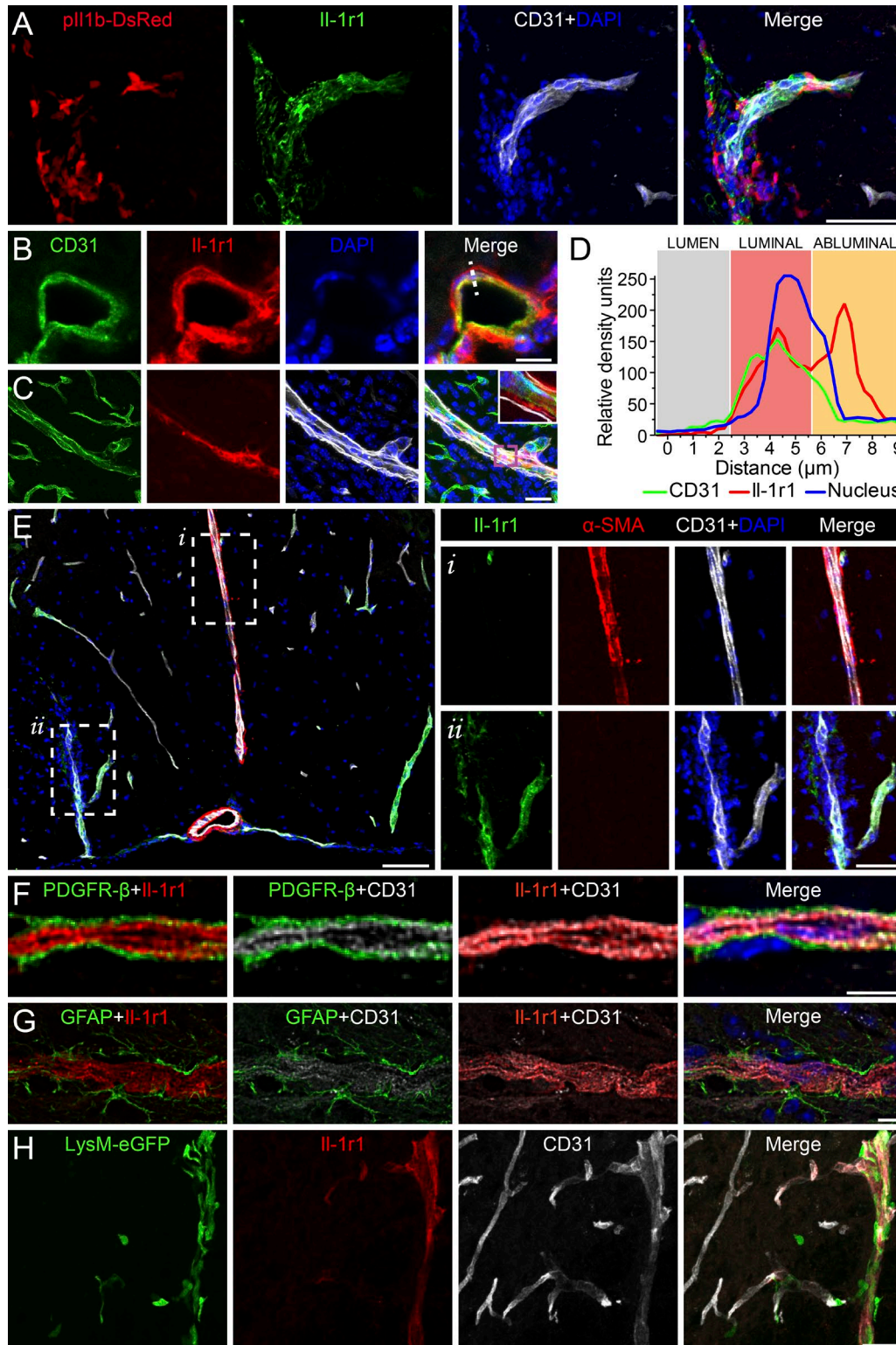


Figure 5. **IL-1 $\beta$  is rarely expressed by spinal cord-resident leptomeningeal macrophages and microglia.** (A) Representative image of the lumbar spinal cord of a CX<sub>3</sub>CR1-Cre<sup>ERT2</sup>::Rosa26-TdT mouse shows that leptomeningeal macrophages from the dura, arachnoid, and pia maters are expressing TdT. (B) Immunofluorescence staining of the spinal cord of a CX<sub>3</sub>CR1-Cre<sup>ERT2</sup>::Rosa26-TdT mouse at the peak of EAE disease is shown. IL-1 $\beta$  protein expression and infiltrating myeloid cells (CD11b<sup>+</sup> TdT<sup>-</sup>), as well as resident leptomeningeal macrophages and microglia (CD11b<sup>+</sup> TdT<sup>+</sup>), are shown. (C) Immunofluorescence staining of the spinal cord of a CX<sub>3</sub>CR1-Cre<sup>ERT2</sup>::Rosa26-TdT::LysM-GFP triple transgenic mouse at the peak of disease. IL-1 $\beta$  and infiltrating myeloid cells (GFP<sup>+</sup> TdT<sup>-</sup>), as well as leptomeningeal macrophages and microglia (GFP<sup>-</sup> TdT<sup>+</sup>), are shown. White arrowheads indicate colocalization with GFP. Bars: (A) 50  $\mu$ m; (B and C) 20  $\mu$ m.

### Adoptive transfer of IL-1 $\beta$ -competent neutrophils and monocytes promotes the recruitment of effector myeloid cells and turns IL-1 $\beta$ KO mice into EAE-sensitive animals

To determine whether the IL-1 $\beta$ -IL-1R1 axis contributes to CNS inflammation and pathology during EAE, we assessed the clinical signs of EAE in normally resistant *Il-1 $\beta$ <sup>-/-</sup>* mice after the transfer of IL-1 $\beta$ -competent neutrophils and monocytes. First, we established that adoptively transferred Gr1<sup>+</sup> (GFP<sup>+</sup>) cells (10:1 neutrophil/monocyte ratio) infiltrated the spinal cord. Several GFP<sup>+</sup> cells expressing CD11b (Fig. 8 A), but not CD3 (Fig. 8 B), were present in the dorsal column of the thoracolumbar spinal cord 1 d after transfer. Using *p11b*-DsRed mice as myeloid cell donors, we confirmed that the transferred Gr1<sup>+</sup> myeloid cells produce pro-IL-1 $\beta$  (Fig. 8 C). In agreement with our hypothesis, the transfer of IL-1 $\beta$ -producing Gr1<sup>+</sup> (GFP<sup>+</sup>) neutrophils and monocytes on the exposed dorsal spinal cord of *Il-1 $\beta$ <sup>-/-</sup>* recipient mice was sufficient to mobilize host-derived (GFP<sup>-</sup>) leukocyte populations

composed mainly of CD11b<sup>+</sup> myeloid cells (Fig. 8 A) and, to a lesser extent, CD3<sup>+</sup> T cells to the area (Fig. 8 B). Colocalization experiments revealed that the vast majority of infiltrated host-derived CD3<sup>+</sup> T cells were in close contact with adoptively transferred Gr1<sup>+</sup> cells (Fig. 8 B). Interestingly, host-derived CD11b<sup>+</sup> cells were seen infiltrating IL-1R1<sup>+</sup> blood vessels where Gr1<sup>+</sup> GFP<sup>+</sup> cells were also present (Fig. 8 D). At 7 d after transfer, Gr1<sup>+</sup> GFP<sup>+</sup> myeloid cells could no longer be detected in the spinal cord and immune cell infiltrates were composed solely of host-derived cells (not depicted). At this time, inflammatory foci were scattered throughout the entire thoracolumbar spinal cord. Strikingly, the infiltration of Gr1<sup>+</sup> cells in the spinal cord of immunized *Il-1 $\beta$ <sup>-/-</sup>* mice was sufficient to induce EAE (Fig. 8 E). Disease incidence went from 34% in immunized *Il-1 $\beta$ <sup>-/-</sup>* mice (Table 1) to 56% after transfer of Gr1<sup>+</sup> neutrophils and monocytes. Disease onset was accelerated by 18 d, passing from 31.7  $\pm$  1.9 dpi in *Il-1 $\beta$ <sup>-/-</sup>* mice to 13.7  $\pm$  1 dpi in the Gr1<sup>+</sup> transfer group. WT



**Figure 6. IL-1R1 is expressed by ECs of the pial venous plexus, which corresponds to the primary site of myeloid cell infiltration during acute EAE.** (A–G) Immunofluorescence confocal microscopy of spinal cord tissue sections from EAE C57BL/6 mice. (A) Immunofluorescence was used to assess whether DsRed<sup>+</sup> cells are found in proximity of CD31<sup>+</sup> ECs and IL-1R1<sup>+</sup> blood vessels at onset of EAE. (B and C) IL-1R1 expression on ECs in a naïve (B) and inflamed (C) spinal cord. The inset in C is a closeup image of the purple box. (D) Graph displaying the abluminal localization of IL-1R1 on ECs (white dashed line in B). (E) Confocal microscopy was used to assess colocalization (or lack thereof) of IL-1R1<sup>+</sup> blood vessels with  $\alpha$ SMA, a protein associated with smooth

→ *IL-1β*<sup>-/-</sup> mice more frequently (in 66.7% of cases) developed hindlimb paralysis (i.e., EAE score >2.0) as compared with the *IL-1β*<sup>-/-</sup> → *IL-1β*<sup>-/-</sup> group (only 22.2%; Fig. 8 F). Accordingly, *IL-1β*<sup>-/-</sup> recipient mice transferred with *IL-1β*<sup>-/-</sup> neutrophils and monocytes had fewer foci of host-derived myeloid (CD11b<sup>+</sup> GFP<sup>-</sup>) cells in the spinal cord as compared with WT → *IL-1β*<sup>-/-</sup> at 7 d after transfer (Fig. 8 G). As expected, unimmunized WT mice that underwent sham surgery plus myeloid cell transfer did not exhibit any symptoms (not depicted). These findings indicate that transferred Gr1<sup>+</sup> cells exert a paracrine IL-1β-dependent stimulation of CNS resident cells (e.g., ECs) to promote the recruitment of effector leukocytes into the CNS. Altogether, our data suggest that IL-1β produced by infiltrating myeloid cells acts on CNS ECs in a paracrine manner to trigger neuroinflammation driving spinal cord pathology during EAE.

## DISCUSSION

IL-1 is one of the most important cell differentiation factors for T<sub>H</sub>17 lymphocytes (Sutton et al., 2006), a population of effector cells required for the development of EAE (Stockinger and Veldhoen, 2007). IL-1 confers encephalitogenicity to T<sub>H</sub>17 cells by regulating GM-CSF production and the subsequent recruitment of effector myeloid cells into the CNS (Codarri et al., 2011; El-Behi et al., 2011). Accordingly, this study and others reported that *IL-1r1*<sup>-/-</sup> mice fail to develop EAE (Schiffenbauer et al., 2000; Sutton et al., 2006; Lukens et al., 2012). Yet, there are studies suggesting that IL-1 signaling may contribute to neural repair by regulating oligodendrocyte lineage development (Mason et al., 2001; Vela et al., 2002). Thus, the exact role of IL-1 in the pathogenesis of animal models of MS remains unclear and contradictory. In this study, we found that production of IL-1β by neutrophils and MDMs after migration across the CNS endothelium is a critical step in EAE pathogenesis. Interestingly, leukocyte infiltrates at the onset of EAE were primarily located around meningeal and parenchymal IL-1R1<sup>+</sup> vessels. We also found that upon stimulation with IL-1β, ECs of the CNS produce a cytokine profile that enhances neuroinflammation and neuropathology by promoting the recruitment of additional effector myeloid cells and subsequent infiltration of T lymphocytes into the CNS.

The mechanisms by which IL-1 induces neuroinflammation during EAE remain poorly defined. IL-1α was recently identified as a DAMP released by dying microglia to induce sterile neuroinflammation after spinal cord injury (Bastien et al., 2015), whereas the IL-1/IL-1Rα systems was shown to play a crucial role in EAE pathogenesis (Matsuki et al., 2006). However, unless the pro-piece of the IL-1α precursor, which is expressed in *IL-1α*<sup>-/-</sup> mice (Horai et al., 1998),

somehow regulates inflammation, IL-1α does not appear to be involved in the induction of autoimmune EAE. Rather, IL-1β alone is required for the development of autoimmune responses within the CNS. Recent studies have implicated IL-1β-dependent production of GM-CSF as a critical factor in T<sub>H</sub>17- and T<sub>H</sub>1-mediated EAE (Codarri et al., 2011; El-Behi et al., 2011). Although these studies suggest a direct effect of IL-1β on T cells, the hypothesis that IL-1β may indirectly contribute to EAE by acting on ECs cannot be ruled out. In fact, it was suggested that endothelial IL-1R1 determines EAE severity (McCandless et al., 2009; Li et al., 2011). In particular, McCandless et al. (2009) showed that IL-1β regulates the localization of Cxcl12 from the abluminal (basolateral) to the luminal side of the spinal cord microvasculature during the induction phase of EAE. In a previous study, the authors demonstrated that redistribution of CXCL12 toward the vessel lumen correlated with CXCR4 activation in leukocytes infiltrating active MS lesions (McCandless et al., 2008). In this study, we found that a subset of ECs associated with CNS postcapillary venules express IL-1R1 and respond to IL-1β during EAE. These findings associate IL-1β-regulated molecules with the pathogenicity of EAE.

Our study is in agreement with results of Li et al. (2011) and suggests that endothelial IL-1R1 is absolutely critical in the development of active EAE. In contrast, in passive EAE, the infusion of WT splenocytes stimulated with IL-1, IL-23, and MOG<sub>35-55</sub> is sufficient to induce disease in *IL-1r1*<sup>-/-</sup> mice (Sutton et al., 2006). It is not clear how passively transferred in vitro-generated T cells bypass the requirement for activation of endothelial IL-1R1 to induce EAE, but this may be attributed to the cytokine cocktail used to induce T<sub>H</sub> cell differentiation. A detailed microarray analysis comparing the transcriptomes of T<sub>H</sub>0 cells differentiated in vitro in the presence of various cytokine cocktails has shown that as many as 434 genes are either up- or down-regulated when co-stimulated with IL-1β, IL-6, and IL-23 to generate T<sub>H</sub>17 cells (Lee et al., 2012). Interestingly, the transfer of T<sub>H</sub>17 cells into naive syngeneic recipient mice was found to induce the production of Cxcl1, Cxcl2, and G-CSF in the spinal cord and to promote neutrophil infiltration (Carlson et al., 2008; Kroenke et al., 2008). Thus, the cytokines involved in T<sub>H</sub> cell differentiation may indirectly influence leukocyte adherence to and transmigration across the CNS endothelium, making the adoptive transfer model less appropriate to identify mechanisms by which the CNS endothelium regulates immune cell entry and reactivation.

We found that both mouse and human CNS-derived ECs exposed to IL-1β express a signature of proinflammatory cytokines (GM-CSF, G-CSF, and IL-6) and chemokines (Cxcl1, Cxcl2, Cxcl5, and Ccl2) that support a pathogenic

---

muscle cells in the tunica media of the artery wall (see insets). (F and G) Triple immunofluorescence staining was performed to assess colocalization of IL-1R1 with CD31, PDGFR-β (pericytes), or GFAP (astrocytes). (H) Myeloid cells (LysM-GFP<sup>+</sup>) were seen to infiltrate almost exclusively through IL-1R1<sup>+</sup> blood vessels. Bars: (A) 10 μm; (B and H) 25 μm; (E insets) 50 μm; (E) 100 μm; (F and G) 5 μm.

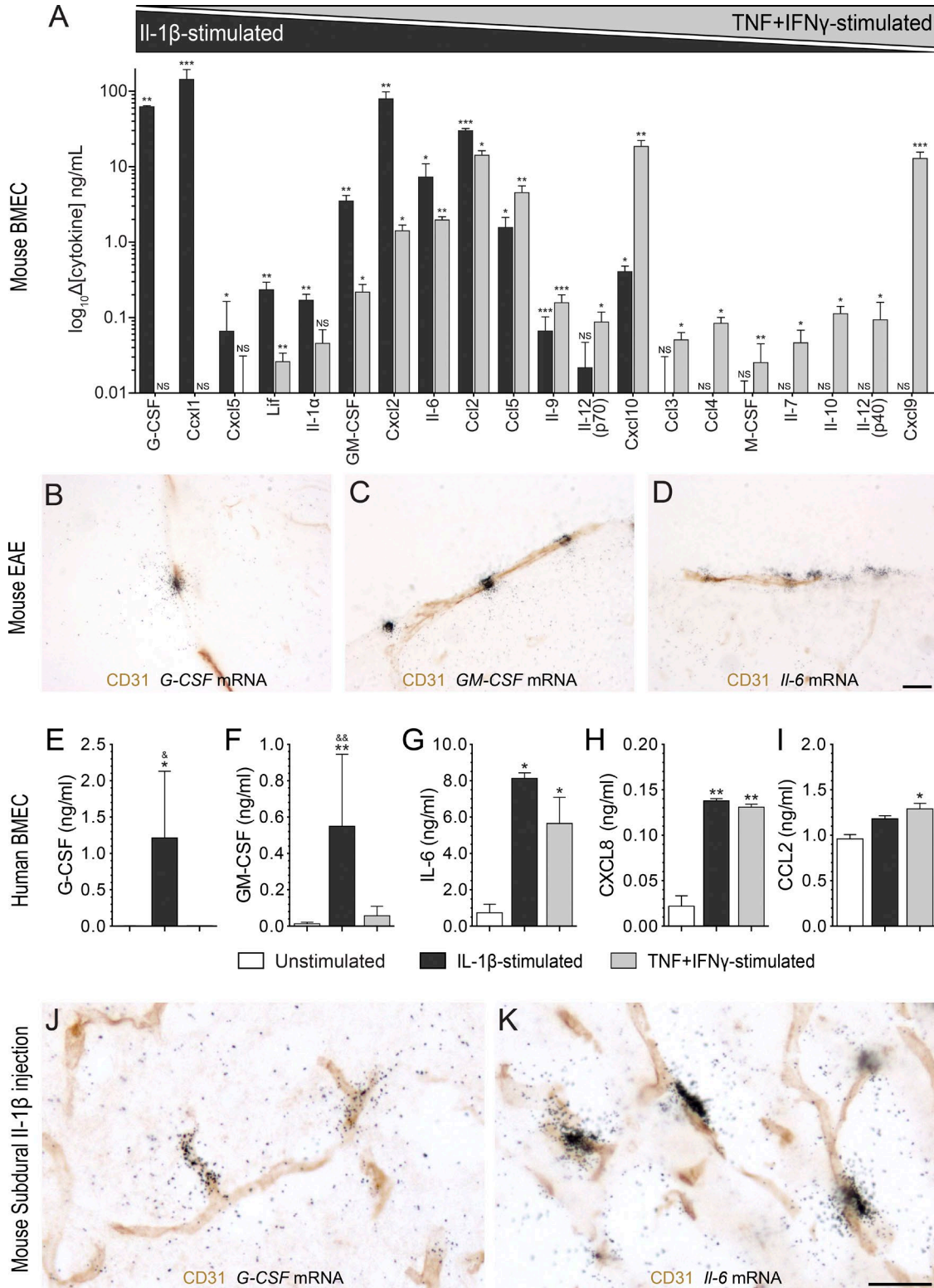


**Figure 7. IL-1 $\beta$  drives a cytokine/chemokine expression profile in mouse and human blood-brain barrier/BSCB ECs predicted to favor neutrophil and monocyte activities.** (A) Cytokine levels in conditioned media collected from primary BMECs treated with IL-1 $\beta$  or TNF + IFN- $\gamma$  as measured using a multiplex ELISA cytokine/chemokine array. Differences compared with the control condition, i.e., culture medium in the absence of cytokine treatment, are expressed in ng/ml for cells stimulated with either 10 ng/ml of recombinant mouse IL-1 $\beta$  (black bars;  $n = 3$ ) or a combination of TNF and IFN- $\gamma$  (gray bars;

role for myeloid cells in EAE. These cytokines and chemokines may contribute to neuroinflammation and autoimmunity by promoting the recruitment of bone marrow-derived cells, such as neutrophils and monocytes, and their maturation into APCs (Ifergan et al., 2008; Geng et al., 2013; Matsushima et al., 2013). Alternatively, neutrophils that infiltrate the CNS of EAE mice may secrete factors that mediate the maturation of APCs within the CNS compartment (Steinbach et al., 2013). Although the exact identity of these neutrophil-secreted cytokines remains unknown, several candidates have been ruled out, including TNF, IL-6, IL-12, and IFN- $\gamma$ . It is interesting to note that, with the exception of IL-6, none of these factors are among the list of cytokines and chemokines up-regulated by ECs after IL-1 $\beta$  treatment. Strikingly, the absence or neutralization of nearly all aforementioned IL-1 $\beta$ -driven cytokines/chemokines was found to prevent or alleviate EAE symptoms, as demonstrated by the following studies: GM-CSF (McQualter et al., 2001; Kroenke et al., 2008, 2010; Codarri et al., 2011; El-Behi et al., 2011), IL-6 (Eugster et al., 1998; Okuda et al., 1998; Samoiloova et al., 1998), Ccl2 (Huang et al., 2001), and Cxcl1 (Roy et al., 2012). No study has investigated the genetic deletion of G-CSF, Cxcl2, and Cxcl5 in EAE, but the Segal group has reported that mice are protected after blockade or in the absence of Cxcr2 (Carlson et al., 2008; Kroenke et al., 2010). In relapsing MS patients, levels of GM-CSF, G-CSF, IL-6, CCL2, CXCL1, CXCL5, and CXCL8 are elevated in the plasma and/or cerebrospinal fluid as compared with healthy subjects, and this increase correlates with lesion burden and MS severity (Carrieri et al., 1998; Ishizu et al., 2005; Campbell et al., 2010; Matsushita et al., 2013; Rumble et al., 2015). Together, these results suggest that cytokines and chemokines released by ECs in response to IL-1 $\beta$  activation play a critical role in the pathogenesis of EAE and MS by regulating the activity of neutrophils and monocytes.

A previous study has suggested that T cells are an important source of IL-1 $\beta$  in EAE (McCandless et al., 2009). However, our results clearly demonstrate that neutrophils and MDMs, but not lymphocytes, produce pro-IL-1 $\beta$  and express the IL-1 $\beta$ -converting enzyme Casp-1. We also show that contrary to the general assumption, resident microglia and leptomeningeal macrophages, which have been until now difficult to distinguish from infiltrating MDMs, express little IL-1 $\beta$  during EAE. It is rather the cells that are committed to the granulocyte-myelomonocytic lineage that produce pro-IL-1 $\beta$  after transmigration across the inflamed CNS endothelium. Likewise, Takashima and colleagues have reported

that neutrophils and MDMs migrating to inflammatory sites express high levels of pro-IL-1 $\beta$  compared with unemigrated cells (Matsushima et al., 2010; Yao et al., 2015). In addition, production of pro-IL-1 $\beta$  can be used as a marker of primed cells characterized by accelerated motility and increased expression of phagocytic receptors (Yao et al., 2015). Whether a paracrine communication loop involving secretion of IL-1 $\beta$  by infiltrated neutrophils and MDMs that would then activate IL-1R1<sup>+</sup> ECs to secrete cytokines known to promote differentiation and maturation of myeloid cells into cells with antigen-presenting capacity is currently under investigation.

This study also unveiled that not all blood vessels in the CNS express IL-1R1, suggesting that a paracrine signaling mechanism only applies to a subpopulation of vessels. Indeed, our results show that IL-1R1 expression is highly enriched in venules and veins that are known as the primary site of leukocyte entry during EAE (Holman et al., 2011). Moreover, Liu et al. (2015) found that ECs are the main producers of IL-1R1 in the CNS and that IL-1R1<sup>+</sup> ECs are present in medium-size blood vessels and are responsible for the effects of centrally administered IL-1 $\beta$  on cyclooxygenase-2 expression, leukocyte infiltration, and global microglia activation. We also found that the endothelial basement membrane of venular vessels expressed IL-1R1, which is not surprising given that the endothelial basement membrane is generated by both ECs and pericytes (Nourshargh et al., 2010). Although CNS pericytes are embedded within the endothelial basement membrane of small- and medium-size veins as well as postcapillary venules (Krueger and Bechmann, 2010; Dalkara et al., 2011), our immunohistochemical analysis provides evidence that IL-1R1 is not expressed by these cells. In the inflamed cremaster muscle, IL-1R1 regulates a leukocyte adhesion cascade that supports subendothelial trafficking of neutrophils along pericyte processes and full breaching of venular walls (Proebstl et al., 2012). In principle, these effects could be extended to other myeloid cell types as they were shown to occur in a CD11b-, ICAM-1-, and LFA-1-dependent manner. Using 2P-IVM, we previously demonstrated that neutrophils mediate early breaches in the BSCB during EAE and established that IL-1R1 governs the firm adhesion of neutrophils to the inflamed spinal cord vasculature (Aubé et al., 2014). Together, these results suggest that endothelial IL-1R1 is a key regulator of myeloid cell trafficking and infiltration during EAE.

In summary, we demonstrated that mice in which IL-1R1 is deleted from radioresistant cells develop a late and less severe form of EAE. Similarly, the manifestation and severity

*n* = 3). (B–D) The combination of immunohistochemistry for the endothelial marker CD31 with ISH for the detection of *G-CSF* (B), *GM-CSF* (C), and *IL-6* (D) mRNAs in the spinal cord of C57BL/6 mice at EAE onset is shown (*n* = 4). (E–I) Cytokines released by primary human BMECs after treatment with either 10 ng/ml of recombinant human IL-1 $\beta$  (black bars) or 100 U TNF + IFN- $\gamma$  (gray bars). Levels of G-CSF (E) GM-CSF (F), IL-6 (G), CXCL8 (H), and CCL2 (I) are means  $\pm$  SEM of experiments from two to five different primary cultures. (J and K) Immunohistochemistry against endothelial CD31 was combined with ISH for *G-CSF* (J) and *IL-6* (K) mRNAs in spinal cord tissue sections from C57BL/6 mice (*n* = 4/group) that received a single subdural injection of recombinant IL-1 $\beta$  (J and K) or saline (not depicted). \*, *P* < 0.05; \*\*, *P* < 0.01; \*\*\*, *P* < 0.001 compared with unstimulated cells;  $\delta$ , *P* < 0.05;  $\delta\delta$ , *P* < 0.01 compared with TNF + IFN- $\gamma$  treatment; one-way ANOVA followed by Dunnett's post-hoc test (A and E–I). Bars, 25  $\mu$ m.

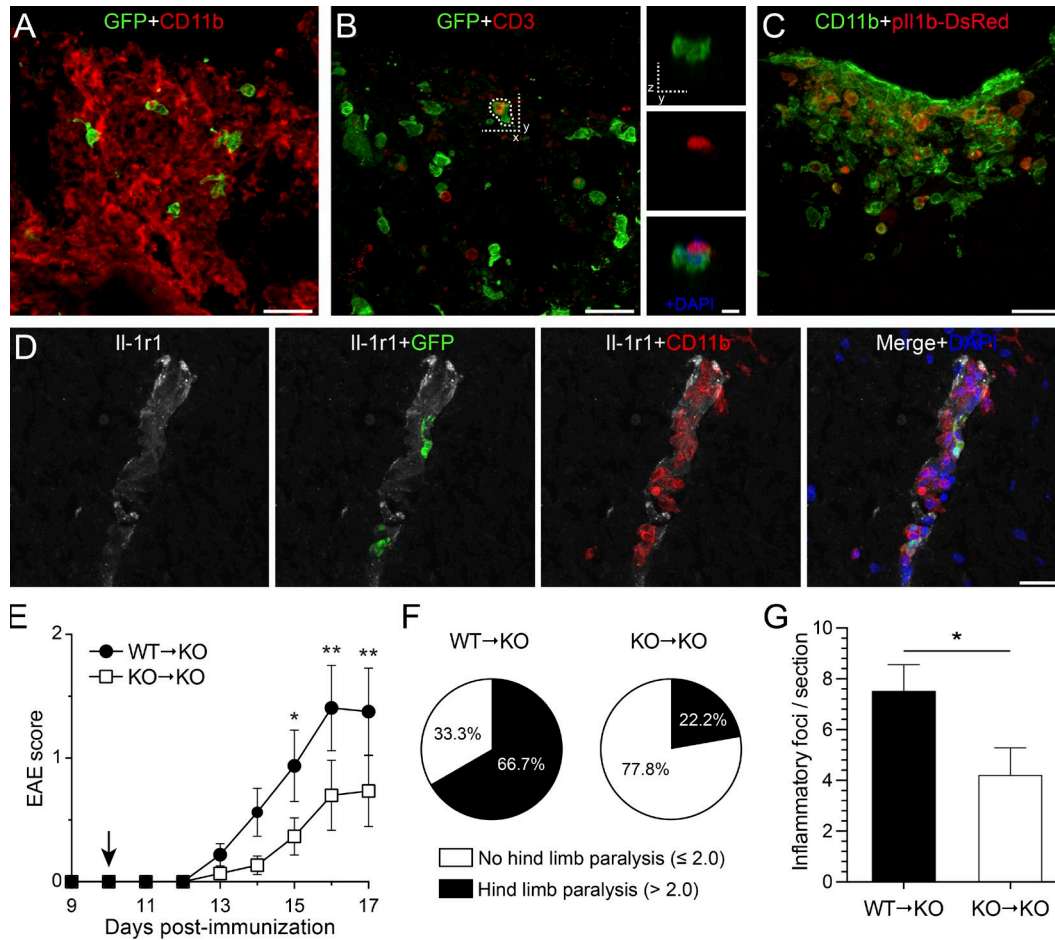


**Figure 8. Adoptive transfer of IL-1-competent neutrophils and monocytes to  $IL-1\beta^{-/-}$  mice induces mobilization of host-derived effector cells into the spinal cord and restores EAE development.** (A–C) Immunofluorescence confocal microscopy of spinal cord tissue sections from immunized  $IL-1\beta^{-/-}$  recipient mice 1 d after the transfer (i.e., at 11 dpi) of  $Gr1^{+}$  neutrophils and monocytes isolated from the bone marrow of IL-1 $\beta$ -competent *LysM-GFP* knock-in (A and B) or *p11b-DsRed* (C) mice. The insets in B are the zoomed-in images of the region delineated with dotted line in B. (D) Immunohistochemical colocalization experiments performed on tissue obtained at 1 d after transfer revealed that host-derived ( $GFP^{+}$ )  $CD11b^{+}$  myeloid cells (red) infiltrated  $IL-1R1^{+}$  vessels (white) where  $Gr1^{+}$   $GFP^{+}$  (green) cells were also present. (E) Clinical course of adoptively transferred EAE into  $MOG_{35-55}$ -immunized IL-1 $\beta$  KO ( $n = 15$ – $16$ /group; data represent two pooled experiments). EAE was scored daily in WT  $\rightarrow$  KO (IL-1 $\beta$  KO recipient mice with neutrophils/monocytes from WT donors) and KO  $\rightarrow$  KO (IL-1 $\beta$  KO recipients with neutrophils/monocytes from IL-1 $\beta$  KO donors) mice up to day 7 after transfer (i.e., 17 dpi). The arrow indicates the time of adoptive transfer of neutrophils/monocytes. (F) Pie charts representing the percentage of animals that displayed hind limb paralysis among mice that developed EAE ( $n = 9$ /group). (G) Quantification of the number of  $CD11b^{+}$  myeloid cell foci in the spinal cord of WT  $\rightarrow$  KO and KO  $\rightarrow$  KO mice at 7 d after transfer ( $n = 9$ – $10$ /group). The data are expressed as mean  $\pm$  SEM. \*,  $P < 0.05$ ; \*\*,  $P < 0.01$  (E–G). Statistical analysis was performed using a two-way repeated-measures ANOVA followed by a Bonferroni post-hoc test (E) or a Student's *t* test (F). Bars: (A–D) 25  $\mu$ m; (insets in B) 10  $\mu$ m.

of EAE symptoms are largely prevented when IL-1 $\beta$  is deleted in bone marrow-derived cells, whereas IL-1 $\alpha$  is dispensable for EAE development. We have demonstrated that most neutrophils and a subset of MDMs, but not T cells, leptomeningeal macrophages, nor microglia, express pro-IL-1 $\beta$  during EAE. Interestingly, we found that synthesis of pro-IL-1 $\beta$  occurs in response to the transendothelial migration of myeloid cells across the inflamed BSCB. We also provided evidence that activation of endothelial IL-1R1 signaling triggers the release of proinflammatory cytokines and chemokines that regulate neutrophil–monocyte recruitment and activation. Fi-

nally, we uncovered that this IL-1 $\beta$ -dependent paracrine loop between infiltrated neutrophils/MDMs and ECs amplifies myeloid cell responses, which are in turn capable of inducing T cell recruitment and CNS pathology. Thus, inhibiting the transmigration of neutrophils and monocytes across the BSCB may be a promising strategy in patients with MS.

## MATERIALS AND METHODS

### Animals

A total of 508 mice of either sex were used in this study. Male and/or female C57BL/6 mice were purchased from

Charles River at 8–10 wk of age. C57BL/6J and IL-1R1 KO mice were purchased from The Jackson Laboratory. All other mouse lines were bred in-house at the Animal Research Facility of the Centre Hospitalier de l'Université Laval (CHUL) Research Center. Breeders for IL-1 $\alpha$  and IL-1 $\beta$  KO mice were obtained from Y. Iwakura (Institute of Medical Science, University of Tokyo, Tokyo, Japan), *pIIIb*-DsRed transgenic mice from A. Takashima (University of Toledo, Toledo, OH), and *LysM-GFP* knock-in mice from G. Dekaban (Robarts Research Institute, London, ON, Canada) with prior authorization from T. Graf (Center for Genomic Regulation, Barcelona, Spain). CX<sub>3</sub>CR1-Cre<sup>ERT2</sup> mice were obtained from the European Mouse Mutant Archive with prior authorization from S. Jung (Weizmann Institute of Science, Rehovot, Israel) and genotyped as previously described (Yona et al., 2013). CX<sub>3</sub>CR1-Cre<sup>ERT2</sup> mice were bred in-house and crossed to Rosa26-TdT mice expressing a loxP-flanked STOP cassette preventing transcription of a CAG promoter-driven RFP variant (TdT). The resulting offspring were termed CX<sub>3</sub>CR1-Cre<sup>ERT2</sup>::Rosa26-TdT mice and treated orally with 10 mg tamoxifen twice at 2-d intervals according to the recommendations of Parkhurst et al. (2013). All experiments were approved by the Animal Welfare Committee of Université Laval in accordance with the Canadian Council on Animal Care policy. All mice had ad libitum access to food and water.

#### Production of chimeric mice

Recipient mice aged 8–10 wk were exposed to a total body  $\gamma$ -irradiation with a single dose of 10 Gy using a cesium-137 source (Gammacell 40 Exactor; MDS Nordion) to destroy hematopoietic stem cells. Within 6 h, mice were injected via the tail vein with  $1.5\text{--}1.8 \times 10^7$  bone marrow cells freshly collected from tibias and femurs of donor mice aged between 2 and 6 mo. In brief, bones were collected from euthanized mice, cleaned of muscle and connective tissue, and then flushed with HBSS + 2% FBS using a 25-gauge needle to harvest bone marrow cells, as previously described (Pineau and Lacroix, 2007). Irradiated mice transplanted with bone marrow cells were housed in autoclaved cages and treated with antibiotics (2.5 ml Septra in 200 ml of drinking water; GlaxoSmithKline) for 1 wk before and 2 wk after irradiation. Animals were housed a total of 8 wk to allow for a complete recovery of the hematopoietic niche. Mice were then immunized to induce EAE as described hereafter.

#### EAE induction and clinical scoring

Mice were immunized by s.c. injections of 100  $\mu$ g MOG<sub>35–55</sub> (MEVGWYRSPFSRVVHLYRNGK; Feldan) emulsified in 100  $\mu$ l of incomplete Freund's Adjuvant supplemented with 4 mg/ml heat-inactivated *Mycobacterium tuberculosis* H37Ra (BD). 200 ng/mouse pertussis toxin (List Biological Laboratories Inc.) was injected i.v. consecutively to MOG<sub>35–55</sub> injections and again 2 d later. Animals were monitored daily to assess weight loss and scored using a grading scale of 0–5 according to the recommendations of Stromnes and Goverman

(2006) as follows: 0 = unaffected, 0.5 = partial limp tail, 1 = paralyzed tail, 1.5 = loss in coordinated movements, 2 = hind limb paresis, 2.5 = one hind limb paralyzed, 3 = both hind limbs paralyzed, 3.5 = hind limbs paralyzed and weakness in forelimbs, 4 = one forelimb paralyzed, 4.5 = both forelimbs paralyzed, and 5 = moribund/death. Mice displaying a score of 2 or higher received daily manual bladder evacuation, and those with a score >3.5 received daily s.c. injections of sterile saline. Mice were killed by exsanguination or by anesthetic overdose at different days after immunization, as indicated.

#### Immunoblotting

Protein extracts of spinal cord, brain, and optic nerve harvested from mice at 0, 1, 3, 7, 10, and 14 dpi were prepared as previously described (de Rivero Vaccari et al., 2012) using antibodies directed against IL-1 $\beta$  (1:10,000; National Cancer Institute) and Casp-1 (1:1,000; Imgenex). Actin (1:10,000; Sigma-Aldrich) was used as a protein loading control and internal standard. Band densities were quantified using the UN-SCAN-IT gel 5.3 software (Silk Scientific Inc.).

#### Leukocyte isolation

**Blood.** Blood was collected with heparinized syringes via cardiac puncture in mice overdosed with a mixture of 400 mg/kg ketamine and 40 mg/kg xylazine. Blood samples were immediately placed in EDTA-coated tubes (Sarstedt Inc.) and gently centrifuged at 5 rpm (LabRoller II) at room temperature until further processing. Mice were then transcardially perfused with ice-cold HBSS to purge remaining blood from the vasculature before collecting femurs, tibias, and the spinal cord.

**Bone marrow.** Femurs and tibias from both legs were collected and bone marrow cells isolated as described above for the production of bone marrow chimeric mice. Erythrocytes were lysed in isotonic solution of ammonium chloride and the remaining cells passed through a 70–100- $\mu$ m nylon mesh and washed twice with PBS + 1% FBS solution. Flow cytometric analysis was performed using total bone marrow cells or enriched neutrophils (see Purification of bone marrow neutrophils and Gr-1<sup>+</sup> cells section).

**Spinal cord.** Spinal cords were dissected out from HBSS-perfused mice and then homogenized with a Potter-Elvehjem tissue grinder. Spinal cord tissue was digested with 3 ml of an enzymatic cocktail containing 0.25% (wt/vol) collagenase type IV (Worthington Biochemical Corporation), 1 U/ml elastase (Worthington Biochemical Corporation), 0.025 U/ml DNase I (Worthington Biochemical Corporation), 0.1  $\mu$ g/ml N $\alpha$ -Tosyl-L-lysine chloromethyl ketone hydrochloride (Sigma-Aldrich), and 20 mM Hepes in HBSS at 37°C for 30 min. After a wash in HBSS, cells were filtered through a 70- $\mu$ m nylon mesh cell strainer (BD), centrifuged at 300 g for 10 min, and washed again with HBSS. Myelin debris was removed by incubating single-cell suspensions with Myelin

Removal Beads II (Miltenyi Biotec) according to the manufacturer's instructions.

### Flow cytometry

Before multicolor immunofluorescent labeling, Fc-receptors were blocked to prevent nonspecific binding using anti-CD16/CD32 mix (BD) in KPBS + 1% FBS for 15 min. Leukocytes were then labeled on ice for 30 min with the following fluorescently conjugated primary antibodies (all from BD except where noted): anti-CD45 PerCP (1:100 dilution), anti-CD11b Alexa Fluor 700 (1:100), anti-Ly6C v450 (1:167), anti-Ly6G PE-Cy7 (1:100), anti-CD115 (1:100), anti-MHCII (1:100), anti-CD3 (1:100), anti-CD4 (1:100), and anti-CD8 (1:100). Except for blood samples, the LIVEDEAD Fixable Yellow Dead Cell Stain kit (Thermo Fisher Scientific) was used to distinguish live from dead cells.

For all analysis, debris and remaining erythrocytes were discarded according to their forward and side scatter characteristics, after which doublets and dead cells were discarded. Only live CD45-expressing leukocytes were considered. Fluorescence minus one controls were used to establish gating boundaries for every fluorochrome-conjugated antibody of the cocktail (Tung et al., 2007). Blood and bone marrow leukocytes were identified as follows: neutrophils (CD45<sup>hi</sup>, CD11b<sup>+</sup>, CD115<sup>-</sup>, Ly6C<sup>dim</sup>, and Ly6G<sup>+</sup>), MDMs (CD45<sup>hi</sup>, CD11b<sup>+</sup>, CD115<sup>+</sup>, Ly6C<sup>med-hi</sup>, and Ly6G<sup>-</sup>), T lymphocytes (CD45<sup>hi</sup>, CD11b<sup>-</sup>, and CD3<sup>+</sup>), and other nonmyeloid cells (CD45<sup>hi</sup>, CD11b<sup>-</sup>, CD115<sup>-</sup>, Ly6C<sup>-</sup>, and Ly6G<sup>-</sup>). The CD115 marker was omitted from spinal cord analysis as it is cleaved from the cell surface once monocytes enter the CNS parenchyma. Microglia were identified as CD45<sup>dim</sup> CD11b<sup>+</sup> CD3<sup>-</sup> Ly6G<sup>-</sup>. Data were acquired with a Special Order Research Product (SORP) flow cytometer (LSR II; BD) and analyzed with FlowJo software (version 10.0.7; Tree Star).

### Real-time quantitative RT-PCR

*Ill1b* and *Casp-1* mRNA expression was examined in leukocyte populations that infiltrated the spinal cord of *pIll1b*-DsRed transgenic mice. DsRed<sup>+</sup> and DsRed<sup>-</sup> neutrophils, MDMs, and T lymphocytes were immunophenotypically distinguished using the markers described in the Flow cytometry section, and sorted based on their expression or lack of expression of DsRed using a SORP flow cytometer (FACSARIA II; BD). Cells were then centrifuged at 700 *g* for 10 min and homogenized in QIAzol buffer (QIAGEN), and total RNA was extracted using the RNeasy Micro kit with on-column DNase digestion (QIAGEN). First-strand cDNA synthesis was accomplished using 0.2 µg of isolated RNA in a reaction containing 200 U SuperScript III RNase H-Reverse transcription (Thermo Fisher Scientific), 300 ng oligo-dT<sub>18</sub>, 50 ng of random hexamers, 50 mM Tris-HCl, pH 8.3, 75 mM KCl, 3 mM MgCl<sub>2</sub>, 0.5 mM deoxynucleotide triphosphate, 5 mM dithiothreitol, and 40 U Protector RNase inhibitor (Roche) in a final volume of 50 µl. The reaction was incubated at 25°C for 10 min and then at 50°C

for 1 h, and a PCR purification kit (QIAGEN) was used to purify cDNA (Thermo Fisher Scientific). Equal amounts of cDNA were amplified in duplicate in a final volume of 10 µl containing 5 µl of 2× LightCycler 480 SYBR Green I Master (Roche), 0.5 µM of forward and reverse primers, and 2 µl of cDNA (10 ng/µl). The primer pairs were as follows: *Ill1b*, 5'-ACTGAACCTGACCGTACAAAATGCCACCTT TTGACAGTGAT-3' and 5'-CGTCAACTTCAAAGAACA GGT CAT-3'; *Casp-1*, 5'-TGAGGGCAAAGAGGAAGC AATT-3' and 5'-CCTGGGGCCCTTTTTT TAGAGA-3'; *Hprt1*, 5'-AGTTCTGTGGCCATCTGCTTAGTAG-3' and 5'-AAACAACAATCCGCCCAAAGG-3'; and *18S*, 5'-ACTGAACCTGACCGTACACGGTACAGTGAACT GCGAATG-3' and 5'-CCAAAGGAACCATAACTGATT TAATGA-3'. The sequences chosen were selected to match only the intended gene using GeneTools software (BioTools Inc.) and verified by basic local alignment search tool (BLAST) analysis in GenBank. Amplification was performed using the LightCycler 480 (Roche) at the following conditions: 2 min at 50°C and 4 min at 95°C followed by 45 cycles of 10 s at 95°C (denaturation), 10 s at 60°C (annealing), 14 s at 72°C (elongation), and 5 s at 74°C (reading). Amplification efficiencies were validated and normalized to *Hprt1* or *18S*, and relative amounts of mRNA levels were calculated using the standard curve method.

### 2P-IVM

2P-IVM was performed in *LysM-GFP::pIll1b*-DsRed at different times after immunization to visualize when and where expression of pro-IL-1β occurs in cells and spinal cord tissue. Animals were anesthetized with 1–2% isoflurane (vol/vol) and a small laminectomy performed at the L1–L2 vertebral level to expose the lumbar spinal cord. The dura mater was removed using the tip of a 27-gauge needle and the spinal cord kept moist afterward using sterile HBSS without Ca<sup>2+</sup>/Mg<sup>2+</sup> (Thermo Fisher Scientific). Mice were then transferred to a custom-made stabilization device adapted for 2P-IVM (Soulet et al., 2013), and body temperature was maintained at 37°C using a temperature controlling device (RWD Life Science Co.). Labeling of blood vessels was achieved through tail vein injection of Qdot 705 (Qtracker 705; 1% wt/vol in saline; Thermo Fisher Scientific). The lumbar spinal cord region to image was next placed under the 25× objective, and Gel-Seal (GE Healthcare) was carefully applied on the bone surrounding the laminectomy to create a watertight cavity. All images were acquired on a two-photon microscope (FV1000; Olympus) and the Mai Tai DeepSee laser (Spectra-Physics) was tuned at a wavelength of 840 nm to simultaneously visualize eGFP, DsRed, and Qdot705. Acquisition parameters were adjusted with the FluoView software (version 3.0a) to capture blood circulating cells or infiltrated cells, i.e., 320 × 320 pixels at 2 µs/pixel or 512 × 512 pixels at 4 µs/pixel, respectively. Images were acquired as time lapses or z-stacks with 2-µm increments, exported into TIFF format, and processed with the Intravital\_Microscopy\_Toolbox

to remove motion artifacts (Soulet et al., 2013). To quantify DsRed expression in individual cells, the perimeter of each eGFP<sup>+</sup> cell was manually drawn in ImageJ (version 1.44o; National Institutes of Health) and saved in separate files. Channels were then separated into eight-bit images, and each individual drawing was imported, and the mean gray value of both the green (eGFP) and red (DsRed) channels were measured in individual cells using ImageJ. Data are presented as a ratio of the intensity of DsRed to eGFP and referred hereafter as DsRed intensity.

#### Purification of bone marrow neutrophils and Gr1<sup>+</sup> cells

Neutrophils were purified from the bone marrow of EAE mice 7 d after MOG<sub>35–55</sub> immunization. Bone marrow cells were collected as described in the Leukocyte isolation/Bone marrow subsection, and neutrophils were isolated using two consecutive Percoll gradients of 64.8% and 61.5%, respectively. Neutrophils were then washed in culture medium, and their purity was assessed using flow cytometry, as described in the Flow cytometry section. The mean neutrophil purity from bone marrow preparations was 95 ± 1% for both WT and *Il-1β*<sup>-/-</sup>.

Bone marrow Gr1<sup>+</sup> cells were purified using the Myeloid-Derived Suppressor Cell Isolation kit (Miltenyi Biotec). In brief, bone marrow cells were extracted from MOG<sub>35–55</sub>-immunized *LysM-GFP* knock-in and *LysM-GFP::Il-1β*<sup>-/-</sup> mice as described in the Leukocyte isolation/Bone marrow subsection and placed in ice-cold HBSS (without Ca<sup>2+</sup>/Mg<sup>2+</sup>). Erythrocytes were lysed using a solution composed of one part Tris-HCl 1 M and nine parts ammonium chloride 0.83%. Gr1<sup>+</sup> cells were labeled and magnetically separated according to the manufacturer's instructions. Gr1<sup>+</sup> (GFP<sup>+</sup>) cells were diluted at a concentration of 10<sup>8</sup> cells/ml in cold PBS (without Ca<sup>2+</sup>/Mg<sup>2+</sup>).

#### Intravital visualization of neutrophils firm attachment

Neutrophils were purified from the bone marrow of EAE mice at 10 dpi as described in the Purification of bone marrow neutrophils and Gr1<sup>+</sup> cells section. Neutrophils were stained for 30 min with the CellTracker green fluorescent probe (1:2,000 dilution; Thermo Fisher Scientific), washed with HBSS, resuspended in sterile saline at a final concentration of 10<sup>6</sup> cells per 200 μl of volume, and then systemically injected via the tail vein. A total of three injections were made (each injected over 1 min) at 2-min intervals in C57BL/6 mice at EAE onset (10–12 dpi). Firmly adherent neutrophils were identified as fluorescent cells stuck to a vessel wall without moving or detaching from the endothelium. Firm neutrophil adhesion was quantified at 10, 30, and 60 min after the first injection in eight different fields of view (25× magnification) containing a sufficient number of postcapillary venules as previously described (Aubé et al., 2014). Importantly, the fields of view were selected before performing the first injection and contained approximately the same number of postcapillary venules.

#### Subdural IL-1β injection and adoptive transfer of Gr1<sup>+</sup> cells

In the experiment in which we studied the effect of IL-1β treatment on cytokine/chemokine expression by cells forming the BSCB, C57BL/6 mice were injected once subdurally at the T10 vertebral level with 100 ng of recombinant mouse IL-1β (R&D Systems) in 2 μl saline using a pulled-glass micropipette connected to a 10-μl Hamilton syringe. Mice were killed 1 d after injection by exsanguination followed by transcardiac perfusion with paraformaldehyde (PFA).

For the experiment in which a mixture of neutrophils and monocytes were transferred onto the spinal cord surface, *Il-1β*<sup>-/-</sup> recipient mice were anesthetized with isoflurane at 10 dpi and a laminectomy performed at the T10 vertebral level. The dura was removed using the tip of a 28<sup>1/2</sup>G needle (insulin syringe) and 10<sup>6</sup> Gr1<sup>+</sup> cells isolated from the bone marrow of either *LysM-GFP* knock-in or *LysM-GFP::Il-1β*<sup>-/-</sup> mice at 10 dpi were placed directly on the exposed dorsal spinal cord surface. The cell suspension was left undisturbed for 1 min, muscles and skin sutured and mice placed on a heating pad (37°C) until recovery.

#### Immunostaining and histology

Mice were overdosed with ketamine-xylazine and transcardially perfused with cold PBS followed by either 1 or 4% PFA (vol/vol), pH 7.4, at 0, 5, 7, 10, and 14 dpi. Spinal cords were dissected out from vertebral columns, post-fixed overnight at 4°C, and then transferred into PBS + 20% sucrose the day before tissue sectioning. Some spinal cords were left inside the vertebral columns, and a decalcification step was performed right after the post-fixation step, by incubating in 0.5 M EDTA, pH 7.4, replaced every other day for 6 d. The spinal cords enclosed in the backbone were then transferred for 1 d into PBS + 20% sucrose solution and embedded in Shandon M-1 Embedding Matrix (Thermo Fisher Scientific) before sectioning. Depending on the experimental protocol, cervical and lumbar spinal segments were cut in 6–12 series of coronal sections set at a thickness of 14–35 μm using a cryostat or microtome. Sections were immunostained with antibodies listed below according to our published protocol (Barrette et al., 2008).

Primary antibodies used in this study are of the following sources and were used at the indicated dilutions: anti-αSMA (clone 1A5; 1:500 dilution; Sigma-Aldrich), anti-CD3e (clone 17A2, 1:1,000; BD), anti-CD4 (clone RM4-5, 1:1,000; Cedarlane), anti-CD31 (clone MEC 13.3; 1:1,000; BD), anti-Desmin (catalog # ab15200; 1:750; Abcam), anti-GFAP (catalog # Z0334; 1:750; Dako), anti-GFP (catalog # A11122; 1:3,000; Thermo Fisher Scientific), anti-Iba-1 (1:750; Wako Pure Chemical Industries), anti-IL-1β (catalog # AF-401NA; 1:100; R&D Systems), anti-IL-1R1 (catalog # AF771; 1:100; R&D Systems), anti-Laminin (catalog # Z0097, 1:1,000; Dako), anti-Ly-6B.2 (clone 7/4; 1:800; AbD Serotec), anti-Ly6G (clone 1A8; 1:2,000; BD), anti-MHCII I-A/I-E (clone M5/114.15.2; 1:2,000; BD), anti-NG2 (catalog # AB5320; 1:250; EMD Millipore), and anti-PDGFR-β (clone Y92; 1:750; Abcam). Alexa Fluor secondary antibody conjugates (1:500; Thermo Fisher

Scientific) were used as secondary antibodies, whereas DAPI (Thermo Fisher Scientific) was used for nuclear counterstaining. To identify arteries and arterioles, sections were either stained with the artery-specific fluorescent dye Alexa Fluor 633 hydrazide according to the methods of Shen et al. (2012), or labeled using anti- $\alpha$ SMA. Sections were observed and imaged on an inverted confocal microscope system (IX81; Olympus) equipped with Diode 405, Ar 488, HeNe1 543, and HeNe2 633 laser lines (Olympus). Quantitative analysis of colocalization for DsRed and markers of immune cell types (Ly6G, Iba1, and CD3) was performed using Fiji software (ImageJ). For each EAE mouse, double-positive cells were counted on at least 15 confocal images showing immune cell infiltration. The results are shown as the percentage of cells expressing DsRed.

### ISH

ISH was performed as previously reported (Vallières et al., 2006). In brief, animals were perfused with ice-cold saline followed by 4% PFA, pH 9.5, in Borax buffer. Spinal cords were removed, post-fixed for 2 d in 4% PFA, and subsequently transferred in a solution of 4% PFA with 10% sucrose for 24 h. Spinal cords were divided into three 4-mm segments corresponding to the thoracic and lumbar spine, sliced into 30- $\mu$ m-thick coronal sections, and collected directly onto Surgipath X-tra microslides (Leica Biosystems). All sections were prehybridized, hybridized, and post-hybridized as described previously (Vallières et al., 2006). To efficiently detect the different mRNAs, the riboprobes were transcribed from linearized cDNAs in the presence of both [ $^{35}$ S]-UTP and [ $^{35}$ S]-CTP (PerkinElmer). Full-length cDNAs coding for the mouse GM-CSF (also known as Csf2) and IL-6 cloned into in vitro transcription vectors are described elsewhere (Pineau and Lacroix, 2007). The full-length cDNA coding for G-CSF (Csf3) was amplified from a mouse spinal cord cDNA library, using the following primers: G-CSF forward, 5'-GCATCGAATTCCAAGAAGCTAACATGTGTGCAGAC-3'; and reverse, 5'-GGTCACTCGAGGCTATACTGCCTTCCAAGTCGTGCTG-3'. The sequences chosen for riboprobe synthesis were selected to match only the intended genes, as verified by BLAST analysis in GenBank. For the combination of immunohistochemistry and ISH, sections were successively incubated for 2 h in blocking buffer (0.5% BSA, 0.04% Triton X-100 and 2.5 mg/ml heparin in PBS) containing the unconjugated anti-CD31 primary antibody (1:500), biotinylated secondary antibody for 1 h, and the avidin-biotinylated horseradish peroxidase complex (ABC) solution (Vector Laboratory) for 1 h. After multiple washes, blood vessels were detected using diaminobenzidine (Sigma-Aldrich). Sections were then prehybridized, hybridized, and post-hybridized. All ISH images were acquired at 40 $\times$  magnification using the Bioquant Nova Prime software on video images of tissue sections transmitted by a high-resolution Retiga QICAM fast color 1394 camera (1,392  $\times$  1,040 pixels; QImaging) installed on a microscope (Eclipse 80i; Nikon). All files were exported as TIFF.

### Isolation and culture of BMECs

**Mouse BMECs.** Primary cultures of mouse BMECs were prepared from adult C57BL/6 mice as we previously described (Aubé et al., 2014) and grown in DMEM supplemented with 20% (vol/vol) FBS, 1 ng/ml basic fibroblast growth factor, 100  $\mu$ g/ml heparin, 1.4  $\mu$ M hydrocortisone, and 1 $\times$  antibiotic-antimycotic solution. The media was changed every day for the first 3 d. 10  $\mu$ g/ml puromycin was added to the media for the first 2 d of culture. On the third day, media was changed for fresh culture media containing 4  $\mu$ g/ml puromycin. On the fifth day, cells were gently washed and media without puromycin containing either recombinant mouse IL-1 $\beta$  (0.1 or 10 ng/ml; R&D Systems) or a combination of TNF + IFN- $\gamma$  (100 U/ml of each; R&D Systems) was added. Supernatants were collected 18 h later, aliquoted, and rapidly stored at -80°C until further use. For the transmigration assay, 5  $\times$  10<sup>4</sup> BMECs were plated on 3- $\mu$ m pore-sized gelatin-coated Boyden chambers and allowed to reach confluence (4 d) before being used.

**Human BMECs.** Primary cultures of human BMECs were prepared from temporal lobe tissue obtained during surgical resection in patients suffering from epilepsy, as previously described (Ifergan et al., 2008). Informed consent and ethical approval were obtained before surgery (Ethical Approval Number BH07.001 to A. Prat). BMECs were grown in medium composed of M199 (Thermo Fisher Scientific) supplemented with 10% FBS, 5% normal human serum, 1.95  $\mu$ g/ml EC growth supplement, and insulin-transferrin-selenium premix on 0.5% gelatin-coated tissue culture plates (all reagents from Sigma-Aldrich unless otherwise indicated). Astrocyte-conditioned media (prepared as before [Ifergan et al., 2008]) was added to the BMEC culture media 24 h before the stimulation with recombinant human cytokines (IL-1 $\beta$  at 0.1 or 10 ng/ml or a combination of TNF and IFN- $\gamma$  at 100 U/ml each; all from R&D Systems).

### Myeloid cell transmigration assay

For the transmigration assay, 10<sup>6</sup> Gr1<sup>+</sup> cells harvested from the bone marrow of naive *p11b*-DsRed mice and magnetically sorted as described in the Purification of bone marrow neutrophils and Gr1<sup>+</sup> cells section were placed in the upper reservoir. 18 h later, cells were collected from the upper and lower chambers, and DsRed expression was analyzed by flow cytometry.

### Multiplex cytokine assay and ELISA

Cytokines released by mouse BMECs stimulated with either IL-1 $\beta$  or TNF + IFN- $\gamma$  were measured using a multiplex laser bead assay (Mouse Cytokine 32-Plex Discovery Assay; Eve Technologies). For primary cultures of human BMECs, levels of released GM-CSF, G-CSF, IL-6, CCL2 (also known as MCP-1), and CXCL8 (IL-8) were measured using ELISA kits (all from BD except for the human G-CSF [Quantikine ELISA kit; R&D Systems]) according to the manufacturers' instructions.

## Statistical analysis

All data are shown as the mean  $\pm$  SEM. Statistical evaluations were performed with one- or two-way ANOVA. Post-ANOVA comparisons were made using the Dunnett or the Bonferroni correction. All statistical analyses were performed using Prism 6 (GraphPad Software). A p-value  $<0.05$  was considered as statistically significant.

## Online supplemental material

Fig. S1 shows the flow cytometry gating strategy. Fig. S2 shows the confirmation of the specificity of the anti-IL-1 $\beta$  antibody by immunostaining of spinal cord tissue sections from WT and IL-1 $\beta^{-/-}$  mice. Video 1 shows intravital imaging of LysM-eGFP::p11b-DsRed mice before EAE onset. Video 2 shows intravital imaging of LysM-eGFP::p11b-DsRed mice at EAE onset. Online supplemental material is available at <http://www.jem.org/cgi/content/full/jem.20151437/DC1>.

## ACKNOWLEDGMENTS

We thank Nadia Fortin, Martine Lessard, and Nicolas Vallières for their invaluable technical assistance.

This study was supported by an operating grant from the Multiple Sclerosis Society of Canada (MSSC; grant ID number 2446) awarded to S. Lacroix. Salary support was provided by the MSSC (to S.A. Lévesque, A. Paré, and J.I. Alvarez) and the Fonds de recherche du Québec en Santé (to M.-A. Lécuyer, A. Prat, and S. Lacroix).

The authors declare no competing financial interests.

Submitted: 4 September 2015

Accepted: 21 March 2016

## REFERENCES

- Aubé, B., S.A. Lévesque, A. Paré, É. Chamma, H. Kébir, R. Gorina, M.A. Lécuyer, J.I. Alvarez, Y. De Koninck, B. Engelhardt, et al. 2014. Neutrophils mediate blood-spinal cord barrier disruption in demyelinating neuroinflammatory diseases. *J. Immunol.* 193:2438–2454 (PubMed). <http://dx.doi.org/10.4049/jimmunol.1400401>
- Badovinac, V., M. Mostarica-Stojković, C.A. Dinarello, and S. Stojić-Grujić. 1998. Interleukin-1 receptor antagonist suppresses experimental autoimmune encephalomyelitis (EAE) in rats by influencing the activation and proliferation of encephalitogenic cells. *J. Neuroimmunol.* 85:87–95. [http://dx.doi.org/10.1016/S0165-5728\(98\)00020-4](http://dx.doi.org/10.1016/S0165-5728(98)00020-4)
- Barrette, B., M.A. Hébert, M. Filali, K. Lafortune, N. Vallières, G. Gowing, J.P. Julien, and S. Lacroix. 2008. Requirement of myeloid cells for axon regeneration. *J. Neurosci.* 28:9363–9376. <http://dx.doi.org/10.1523/JNEUROSCI.1447-08.2008>
- Bastien, D., V. Bellver Landete, M. Lessard, N. Vallières, M. Champagne, A. Takashima, M.E. Tremblay, Y. Doyon, and S. Lacroix. 2015. IL-1 $\alpha$  gene deletion protects oligodendrocytes after spinal cord injury through upregulation of the survival factor Tox3. *J. Neurosci.* 35:10715–10730. <http://dx.doi.org/10.1523/JNEUROSCI.0498-15.2015>
- Campbell, S.J., U. Meier, S. Mardiguan, Y. Jiang, E.T. Littleton, A. Bristow, J. Relton, T.J. Connor, and D.C. Anthony. 2010. Sickness behaviour is induced by a peripheral CXC-chemokine also expressed in multiple sclerosis and EAE. *Brain Behav. Immun.* 24:738–746. <http://dx.doi.org/10.1016/j.bbi.2010.01.011>
- Cannella, B., and C.S. Raine. 1995. The adhesion molecule and cytokine profile of multiple sclerosis lesions. *Ann. Neurol.* 37:424–435. <http://dx.doi.org/10.1002/ana.410370404>
- Carare, R.O., M. Bernardes-Silva, T.A. Newman, A.M. Page, J.A. Nicoll, V.H. Perry, and R.O. Weller. 2008. Solutes, but not cells, drain from the brain parenchyma along basement membranes of capillaries and arteries: significance for cerebral amyloid angiopathy and neuroimmunology. *Neuropathol. Appl. Neurobiol.* 34:131–144. <http://dx.doi.org/10.1111/j.1365-2990.2007.00926.x>
- Carlson, T., M. Kroenke, P. Rao, T.E. Lane, and B. Segal. 2008. The Th17–ELR<sup>+</sup> CXC chemokine pathway is essential for the development of central nervous system autoimmune disease. *J. Exp. Med.* 205:811–823. <http://dx.doi.org/10.1084/jem.20072404>
- Carpintero, R., and D. Burger. 2011. IFN $\beta$  and glatiramer acetate trigger different signaling pathways to regulate the IL-1 system in multiple sclerosis. *Commun. Integr. Biol.* 4:112–114. <http://dx.doi.org/10.4161/cib.14205>
- Carrieri, P.B., V. Provitera, T. De Rosa, G. Tartaglia, F. Gorga, and O. Perrella. 1998. Profile of cerebrospinal fluid and serum cytokines in patients with relapsing-remitting multiple sclerosis: a correlation with clinical activity. *Immunopharmacol. Immunotoxicol.* 20:373–382. <http://dx.doi.org/10.3109/08923979809034820>
- Codarri, L., G. Gyölvérsi, V. Tosevski, L. Hesske, A. Fontana, L. Magnenat, T. Suter, and B. Becher. 2011. ROR $\gamma$ t drives production of the cytokine GM-CSF in helper T cells, which is essential for the effector phase of autoimmune neuroinflammation. *Nat. Immunol.* 12:560–567. <http://dx.doi.org/10.1038/ni.2027>
- Compston, A. 2004. The pathogenesis and basis for treatment in multiple sclerosis. *Clin. Neurol. Neurosurg.* 106:246–248. <http://dx.doi.org/10.1016/j.clineuro.2004.02.007>
- Dalkara, T., Y. Gurses-Ozdemir, and M. Yemisci. 2011. Brain microvascular pericytes in health and disease. *Acta Neuropathol.* 122:1–9. <http://dx.doi.org/10.1007/s00401-011-0847-6>
- de Jong, B.A., T.W. Huizinga, E.L. Bollen, B.M. Uitdehaag, G.P. Bosma, M.A. van Buchem, E.J. Remarque, A.C. Burgmans, N.F. Kalkers, C.H. Polman, and R.G. Westendorp. 2002. Production of IL-1 $\beta$  and IL-1Ra as risk factors for susceptibility and progression of relapse-onset multiple sclerosis. *J. Neuroimmunol.* 126:172–179. [http://dx.doi.org/10.1016/S0165-5728\(02\)00056-5](http://dx.doi.org/10.1016/S0165-5728(02)00056-5)
- de Rivero Vaccari, J.P., D. Bastien, G. Yurcisin, I. Pineau, W.D. Dietrich, Y. De Koninck, R.W. Keane, and S. Lacroix. 2012. P2X4 receptors influence inflammasome activation after spinal cord injury. *J. Neurosci.* 32:3058–3066. <http://dx.doi.org/10.1523/JNEUROSCI.4930-11.2012>
- Dinarello, C.A. 2009. Immunological and inflammatory functions of the interleukin-1 family. *Annu. Rev. Immunol.* 27:519–550. <http://dx.doi.org/10.1146/annurev.immunol.021908.132612>
- Dinarello, C.A. 2011. Interleukin-1 in the pathogenesis and treatment of inflammatory diseases. *Blood.* 117:3720–3732. <http://dx.doi.org/10.1182/blood-2010-07-273417>
- El-Behi, M., B. Ciric, H. Dai, Y. Yan, M. Cullimore, F. Safavi, G.X. Zhang, B.N. Dittel, and A. Rostami. 2011. The encephalitogenicity of TH17 cells is dependent on IL-1- and IL-23-induced production of the cytokine GM-CSF. *Nat. Immunol.* 12:568–575. <http://dx.doi.org/10.1038/ni.2031>
- Eugster, H.P., K. Frei, M. Kopf, H. Lassmann, and A. Fontana. 1998. IL-6-deficient mice resist myelin oligodendrocyte glycoprotein-induced autoimmune encephalomyelitis. *Eur. J. Immunol.* 28:2178–2187. [http://dx.doi.org/10.1002/\(SICI\)1521-4141\(199807\)28:07<2178::AID-IMMU2178>3.0.CO;2-D](http://dx.doi.org/10.1002/(SICI)1521-4141(199807)28:07<2178::AID-IMMU2178>3.0.CO;2-D)
- Furlan, R., A. Bergami, E. Brambilla, E. Butti, M.G. De Simoni, M. Campagnoli, P. Marconi, G. Comi, and G. Martino. 2007. HSV-1-mediated IL-1 receptor antagonist gene therapy ameliorates MOG<sub>35–55</sub>-induced experimental autoimmune encephalomyelitis in C57BL/6 mice. *Gene Ther.* 14:93–98. <http://dx.doi.org/10.1038/sj.gt.3302805>
- Geng, S., H. Matsushima, T. Okamoto, Y. Yao, R. Lu, K. Page, R.M. Blumenthal, N.L. Ward, T. Miyazaki, and A. Takashima. 2013. Emergence, origin, and

- function of neutrophil-dendritic cell hybrids in experimentally induced inflammatory lesions in mice. *Blood*. 121:1690–1700. <http://dx.doi.org/10.1182/blood-2012-07-445197>
- Holman, D.W., R.S. Klein, and R.M. Ransohoff. 2011. The blood-brain barrier, chemokines and multiple sclerosis. *Biochim. Biophys. Acta*. 1812:220–230. <http://dx.doi.org/10.1016/j.bbdis.2010.07.019>
- Horai, R., M. Asano, K. Sudo, H. Kanuka, M. Suzuki, M. Nishihara, M. Takahashi, and Y. Iwakura. 1998. Production of mice deficient in genes for interleukin (IL)-1 $\alpha$ , IL-1 $\beta$ , IL-1 $\alpha/\beta$ , and IL-1 receptor antagonist shows that IL-1 $\beta$  is crucial in turpentine-induced fever development and glucocorticoid secretion. *J. Exp. Med.* 187:1463–1475. <http://dx.doi.org/10.1084/jem.187.9.1463>
- Huang, D.R., J. Wang, P. Kivisakk, B.J. Rollins, and R.M. Ransohoff. 2001. Absence of monocyte chemoattractant protein 1 in mice leads to decreased local macrophage recruitment and antigen-specific T helper cell type 1 immune response in experimental autoimmune encephalomyelitis. *J. Exp. Med.* 193:713–726. <http://dx.doi.org/10.1084/jem.193.6.713>
- Ifergan, I., H. Kébir, M. Bernard, K. Wosik, A. Dodelet-Devillers, R. Cayrol, N. Arbour, and A. Prat. 2008. The blood-brain barrier induces differentiation of migrating monocytes into Th17-polarizing dendritic cells. *Brain*. 131:785–799. <http://dx.doi.org/10.1093/brain/awm295>
- Ishizu, T., M. Osoegawa, F.J. Mei, H. Kikuchi, M. Tanaka, Y. Takakura, M. Minohara, H. Murai, F. Mihara, T. Taniwaki, and J. Kira. 2005. Intrathecal activation of the IL-17/IL-8 axis in opticospinal multiple sclerosis. *Brain*. 128:988–1002. <http://dx.doi.org/10.1093/brain/awh453>
- Jacobs, C.A., P.E. Baker, E.R. Roux, K.S. Picha, B. Toivola, S. Waugh, and M.K. Kennedy. 1991. Experimental autoimmune encephalomyelitis is exacerbated by IL-1 alpha and suppressed by soluble IL-1 receptor. *J. Immunol.* 146:2983–2989.
- Kroenke, M.A., T.J. Carlson, A.V. Andjelkovic, and B.M. Segal. 2008. IL-12- and IL-23-modulated T cells induce distinct types of EAE based on histology, CNS chemokine profile, and response to cytokine inhibition. *J. Exp. Med.* 205:1535–1541. <http://dx.doi.org/10.1084/jem.20080159>
- Kroenke, M.A., S.W. Chensue, and B.M. Segal. 2010. EAE mediated by a non-IFN- $\gamma$ /non-IL-17 pathway. *Eur. J. Immunol.* 40:2340–2348. <http://dx.doi.org/10.1002/eji.201040489>
- Krueger, M., and I. Bechmann. 2010. CNS pericytes: concepts, misconceptions, and a way out. *Glia*. 58:1–10. <http://dx.doi.org/10.1002/glia.20898>
- Lee, Y., A. Awasthi, N. Yosef, F.J. Quintana, S. Xiao, A. Peters, C. Wu, M. Kleinewietfeld, S. Kunder, D.A. Hafler, et al. 2012. Induction and molecular signature of pathogenic TH17 cells. *Nat. Immunol.* 13:991–999. <http://dx.doi.org/10.1038/ni.2416>
- Lewis, N.D., J.D. Hill, K.W. Juchem, D.E. Stefanopoulos, and L.K. Modis. 2014. RNA sequencing of microglia and monocyte-derived macrophages from mice with experimental autoimmune encephalomyelitis illustrates a changing phenotype with disease course. *J. Neuroimmunol.* 277:26–38. <http://dx.doi.org/10.1016/j.jneuroim.2014.09.014>
- Li, Q., N. Powell, H. Zhang, N. Belevych, S. Ching, Q. Chen, J. Sheridan, C. Whitacre, and N. Quan. 2011. Endothelial IL-1R1 is a critical mediator of EAE pathogenesis. *Brain Behav. Immun.* 25:160–167. <http://dx.doi.org/10.1016/j.bbi.2010.09.009>
- Liu, X., T. Yamashita, Q. Chen, N. Belevych, D.B. Mckim, A.J. Tarr, V. Coppola, N. Nath, D.P. Nemeth, Z.W. Syed, et al. 2015. Interleukin 1 type 1 receptor restore: a genetic mouse model for studying interleukin 1 receptor-mediated effects in specific cell types. *J. Neurosci.* 35:2860–2870. <http://dx.doi.org/10.1523/JNEUROSCI.3199-14.2015>
- Lukens, J.R., M.J. Barr, D.D. Chaplin, H. Chi, and T.D. Kanneganti. 2012. Inflammation-derived IL-1 $\beta$  regulates the production of GM-CSF by CD4<sup>+</sup> T cells and  $\gamma\delta$  T cells. *J. Immunol.* 188:3107–3115. <http://dx.doi.org/10.4049/jimmunol.1103308>
- Mason, J.L., K. Suzuki, D.D. Chaplin, and G.K. Matsushima. 2001. Interleukin-1beta promotes repair of the CNS. *J. Neurosci.* 21:7046–7052.
- Matsuki, T., S. Nakae, K. Sudo, R. Horai, and Y. Iwakura. 2006. Abnormal T cell activation caused by the imbalance of the IL-1/IL-1R antagonist system is responsible for the development of experimental autoimmune encephalomyelitis. *Int. Immunol.* 18:399–407. <http://dx.doi.org/10.1093/intimm/dxh379>
- Matsushima, H., Y. Ogawa, T. Miyazaki, H. Tanaka, A. Nishibu, and A. Takashima. 2010. Intravital imaging of IL-1 $\beta$  production in skin. *J. Invest. Dermatol.* 130:1571–1580. <http://dx.doi.org/10.1038/jid.2010.11>
- Matsushima, H., S. Geng, R. Lu, T. Okamoto, Y. Yao, N. Mayuzumi, P.F. Kotol, B.J. Chojnacki, T. Miyazaki, R.L. Gallo, and A. Takashima. 2013. Neutrophil differentiation into a unique hybrid population exhibiting dual phenotype and functionality of neutrophils and dendritic cells. *Blood*. 121:1677–1689. <http://dx.doi.org/10.1182/blood-2012-07-445189>
- Matsushita, T., T. Tateishi, N. Isobe, T. Yonekawa, R. Yamasaki, D. Matsuse, H. Murai, and J. Kira. 2013. Characteristic cerebrospinal fluid cytokine/chemokine profiles in neuromyelitis optica, relapsing remitting or primary progressive multiple sclerosis. *PLoS One*. 8:e61835. <http://dx.doi.org/10.1371/journal.pone.0061835>
- McCandless, E.E., L. Piccio, B.M. Woerner, R.E. Schmidt, J.B. Rubin, A.H. Cross, and R.S. Klein. 2008. Pathological expression of CXCL12 at the blood-brain barrier correlates with severity of multiple sclerosis. *Am. J. Pathol.* 172:799–808. <http://dx.doi.org/10.2353/ajpath.2008.070918>
- McCandless, E.E., M. Budde, J.R. Lees, D. Dorsey, E. Lyng, and R.S. Klein. 2009. IL-1R signaling within the central nervous system regulates CXCL12 expression at the blood-brain barrier and disease severity during experimental autoimmune encephalomyelitis. *J. Immunol.* 183:613–620. <http://dx.doi.org/10.4049/jimmunol.0802258>
- McGuinness, M.C., J.M. Powers, W.B. Bias, B.J. Schmeckpeper, A.H. Segal, V.C. Gowda, S.L. Wesselingh, J. Berger, D.E. Griffin, and K.D. Smith. 1997. Human leukocyte antigens and cytokine expression in cerebral inflammatory demyelinating lesions of X-linked adrenoleukodystrophy and multiple sclerosis. *J. Neuroimmunol.* 75:174–182. [http://dx.doi.org/10.1016/S0165-5728\(97\)00020-9](http://dx.doi.org/10.1016/S0165-5728(97)00020-9)
- McQualter, J.L., R. Darwiche, C. Ewing, M. Onuki, T.W. Kay, J.A. Hamilton, H.H. Reid, and C.C. Bernard. 2001. Granulocyte macrophage colony-stimulating factor: a new putative therapeutic target in multiple sclerosis. *J. Exp. Med.* 194:873–882. <http://dx.doi.org/10.1084/jem.194.7.873>
- Mellergård, J., M. Edström, M. Vrethem, J. Ernerudh, and C. Dahle. 2010. Natalizumab treatment in multiple sclerosis: marked decline of chemokines and cytokines in cerebrospinal fluid. *Mult. Scler.* 16:208–217. <http://dx.doi.org/10.1177/1352458509355068>
- Miranda-Hernandez, S., N. Gerlach, J.M. Fletcher, E. Biro, M. Mack, H. Körner, and A.G. Baxter. 2011. Role for MyD88, TLR2 and TLR9 but not TLR1, TLR4 or TLR6 in experimental autoimmune encephalomyelitis. *J. Immunol.* 187:791–804. <http://dx.doi.org/10.4049/jimmunol.1001992>
- Nourshargh, S., P.L. Hordijk, and M. Sixt. 2010. Breaching multiple barriers: leukocyte motility through venular walls and the interstitium. *Nat. Rev. Mol. Cell Biol.* 11:366–378. <http://dx.doi.org/10.1038/nrm2889>
- Okuda, Y., S. Sakoda, C.C. Bernard, H. Fujimura, Y. Saeki, T. Kishimoto, and T. Yanagihara. 1998. IL-6-deficient mice are resistant to the induction of experimental autoimmune encephalomyelitis provoked by myelin oligodendrocyte glycoprotein. *Int. Immunol.* 10:703–708. <http://dx.doi.org/10.1093/intimm/10.5.703>
- Parkhurst, C.N., G. Yang, I. Ninan, J.N. Savas, J.R. Yates III, J.J. Lafaille, B.L. Hempstead, D.R. Littman, and W.B. Gan. 2013. Microglia promote learning-dependent synapse formation through brain-derived neurotrophic factor. *Cell*. 155:1596–1609. <http://dx.doi.org/10.1016/j.cell.2013.11.030>
- Pineau, I., and S. Lacroix. 2007. Proinflammatory cytokine synthesis in the injured mouse spinal cord: multiphasic expression pattern and

- identification of the cell types involved. *J. Comp. Neurol.* 500:267–285. <http://dx.doi.org/10.1002/cne.21149>
- Proebstl, D., M.B. Voisin, A. Woodfin, J. Whiteford, F. D'Acquisto, G.E. Jones, D. Rowe, and S. Nourshargh. 2012. Pericytes support neutrophil subendothelial cell crawling and breaching of venular walls in vivo. *J. Exp. Med.* 209:1219–1234. <http://dx.doi.org/10.1084/jem.20111622>
- Rider, P., Y. Carmi, E. Voronov, and R.N. Apte. 2013. Interleukin-1 $\alpha$ . *Semin. Immunol.* 25:430–438. <http://dx.doi.org/10.1016/j.smim.2013.10.005>
- Roy, M., J.F. Richard, A. Dumas, and L. Vallières. 2012. CXCL1 can be regulated by IL-6 and promotes granulocyte adhesion to brain capillaries during bacterial toxin exposure and encephalomyelitis. *J. Neuroinflammation.* 9:18. <http://dx.doi.org/10.1186/1742-2094-9-18>
- Rumble, J.M., A.K. Huber, G. Krishnamoorthy, A. Srinivasan, D.A. Giles, X. Zhang, L. Wang, and B.M. Segal. 2015. Neutrophil-related factors as biomarkers in EAE and MS. *J. Exp. Med.* 212:23–35. <http://dx.doi.org/10.1084/jem.20141015>
- Samoilova, E.B., J.L. Horton, B. Hilliard, T.S. Liu, and Y. Chen. 1998. IL-6-deficient mice are resistant to experimental autoimmune encephalomyelitis: roles of IL-6 in the activation and differentiation of autoreactive T cells. *J. Immunol.* 161:6480–6486.
- Schiffenbauer, J., W.J. Streit, E. Butfiloski, M. LaBow, C. Edwards III, and L.L. Moldawer. 2000. The induction of EAE is only partially dependent on TNF receptor signaling but requires the IL-1 type I receptor. *Clin. Immunol.* 95:117–123. <http://dx.doi.org/10.1006/clim.2000.4851>
- Seppi, D., M. Puthenparampil, L. Federle, S. Ruggero, E. Toffanin, F. Rinaldi, P. Perini, and P. Gallo. 2014. Cerebrospinal fluid IL-1 $\beta$  correlates with cortical pathology load in multiple sclerosis at clinical onset. *J. Neuroimmunol.* 270:56–60. <http://dx.doi.org/10.1016/j.jneuroim.2014.02.014>
- Shen, Z., Z. Lu, P.Y. Chhatbar, P. O'Herron, and P. Kara. 2012. An artery-specific fluorescent dye for studying neurovascular coupling. *Nat. Methods.* 9:273–276. <http://dx.doi.org/10.1038/nmeth.1857>
- Soulet, D., A. Paré, J. Coste, and S. Lacroix. 2013. Automated filtering of intrinsic movement artifacts during two-photon intravital microscopy. *PLoS One.* 8:e53942. <http://dx.doi.org/10.1371/journal.pone.0053942>
- Steinbach, K., M. Piedavent, S. Bauer, J.T. Neumann, and M.A. Friese. 2013. Neutrophils amplify autoimmune central nervous system infiltrates by maturing local APCs. *J. Immunol.* 191:4531–4539. <http://dx.doi.org/10.4049/jimmunol.1202613>
- Stockinger, B., and M. Veldhoen. 2007. Differentiation and function of Th17 T cells. *Curr. Opin. Immunol.* 19:281–286. <http://dx.doi.org/10.1016/j.coi.2007.04.005>
- Stromnes, I.M., and J.M. Goverman. 2006. Active induction of experimental allergic encephalomyelitis. *Nat. Protoc.* 1:1810–1819. <http://dx.doi.org/10.1038/nprot.2006.285>
- Sutton, C., C. Brereton, B. Keogh, K.H. Mills, and E.C. Lavelle. 2006. A crucial role for interleukin (IL)-1 in the induction of IL-17-producing T cells that mediate autoimmune encephalomyelitis. *J. Exp. Med.* 203:1685–1691. <http://dx.doi.org/10.1084/jem.20060285>
- Sutton, C.E., S.J. Lalor, C.M. Sweeney, C.F. Brereton, E.C. Lavelle, and K.H. Mills. 2009. Interleukin-1 and IL-23 induce innate IL-17 production from  $\gamma\delta$  T cells, amplifying Th17 responses and autoimmunity. *Immunity.* 31:331–341. <http://dx.doi.org/10.1016/j.immuni.2009.08.001>
- Tung, J.W., K. Heydari, R. Tirouvanziam, B. Sahaf, D.R. Parks, L.A. Herzenberg, and L.A. Herzenberg. 2007. Modern flow cytometry: a practical approach. *Clin. Lab. Med.* 27:453–468. <http://dx.doi.org/10.1016/j.cl.2007.05.001>
- Vallières, N., J.L. Berard, S. David, and S. Lacroix. 2006. Systemic injections of lipopolysaccharide accelerates myelin phagocytosis during Wallerian degeneration in the injured mouse spinal cord. *Glia.* 53:103–113. <http://dx.doi.org/10.1002/glia.20266>
- Vela, J.M., E. Molina-Holgado, A. Arévalo-Martín, G. Almazán, and C. Guaza. 2002. Interleukin-1 regulates proliferation and differentiation of oligodendrocyte progenitor cells. *Mol. Cell. Neurosci.* 20:489–502. <http://dx.doi.org/10.1006/mcne.2002.1127>
- Williams, M.R., N. Kataoka, Y. Sakurai, C.M. Powers, S.G. Eskin, and L.V. McIntire. 2008. Gene expression of endothelial cells due to interleukin-1 beta stimulation and neutrophil transmigration. *Endothelium.* 15:73–84. <http://dx.doi.org/10.1080/10623320802092443>
- Yao, Y., H. Matsushima, J.A. Ohtola, S. Geng, R. Lu, and A. Takashima. 2015. Neutrophil priming occurs in a sequential manner and can be visualized in living animals by monitoring IL-1 $\beta$  promoter activation. *J. Immunol.* 194:1211–1224. <http://dx.doi.org/10.4049/jimmunol.1402018>
- Yona, S., K.W. Kim, Y. Wolf, A. Mildner, D. Varol, M. Breker, D. Strauss-Ayali, S. Viukov, M. Guilliams, A. Misharin, et al. 2013. Fate mapping reveals origins and dynamics of monocytes and tissue macrophages under homeostasis. *Immunity.* 38:79–91. <http://dx.doi.org/10.1016/j.immuni.2012.12.001>
- Zsebo, K.M., V.N. Yuschenkoff, S. Schiffer, D. Chang, E. McCall, C.A. Dinarello, M.A. Brown, B. Altrick, and G.C. Bagby Jr. 1988. Vascular endothelial cells and granulopoiesis: interleukin-1 stimulates release of G-CSF and GM-CSF. *Blood.* 71:99–103.